

1 **Experimental study of non-Darcian flow characteristics in permeable stones**

2

3

4 A manuscript prepared for *Hydrology and Earth System Sciences*

5 by

6 Zhongxia Li<sup>1</sup>, Junwei Wan<sup>1</sup>, Tao Xiong<sup>1</sup>, Hongbin Zhan<sup>2\*</sup>, Linqing He<sup>3</sup>, Kun Huang<sup>1\*</sup>

7 <sup>1</sup>School of Environmental Studies, China University of Geosciences, 430074 Wuhan, China.

8 <sup>2</sup>Department of Geology and Geophysics, Texas A & M University, College Station, TX

9 77843-3115, USA.

10 <sup>3</sup>Changjiang Institute of Survey Technical Research MWR, Wuhan, China.

11 \* Corresponding authors:

12 Dr. Hongbin Zhan (zhan@tamu.edu);

13 Dr. Kun Huang (cugdr\_huang@cug.edu.cn).

14

15

16

17

18

19

20

## 21 **Abstract**

22 This study provides experimental evidence of Forchheimer flow and transition between  
23 different flow regimes from the perspective of pore size of permeable stone. We have firstly  
24 carried out the seepage experiments of permeable stones with four different mesh sizes,  
25 including 24 mesh size, 46 mesh size, 60 mesh size, and 80 mesh size, which corresponding  
26 to mean particle sizes (50% by weight) of 0.71 mm, 0.36 mm, 0.25 mm, and 0.18 mm. The  
27 seepage experiments show that obvious deviation from Darcian flow regime is visible. In  
28 addition, the critical specific discharge corresponding to the transition of flow regimes (from  
29 pre-Darcian to post-Darcian) increases with the increase of particle sizes. When the “pseudo”  
30 hydraulic conductivity ( $K$ ) (which is computed by the ratio of specific discharge and the  
31 hydraulic gradient) increases with the increase of specific discharge ( $q$ ), the flow regime is  
32 denoted as the pre-Darcian flow. After the specific discharge increases to a certain value, the  
33 “pseudo” hydraulic conductivity begins to decrease, and this regime is called the post-  
34 Darcian flow. In addition, we use the mercury injection experiment to measure the pore size  
35 distribution of four permeable stones with different particle sizes, and the mercury injection  
36 curve is divided into three stages. The beginning and end segments of the mercury injection  
37 curve are very gentle with relatively small slopes, while the intermediate mercury injection  
38 curve is steep, indicating that the pore size in permeable stones is relatively uniform. The  
39 porosity decreases as the mean particle sizes increases, and the mean pore size can faithfully  
40 reflect the influence of particle diameter, sorting degree and arrangement mode of porous  
41 medium on seepage parameters. This study shows that the size of pores is an essential factor  
42 for determining the flow regimes. In addition, the Forchheimer coefficients are also discussed  
43 in which the coefficient  $A$  (which is related to the linear term of the Forchheimer equation) is  
44 linearly related to  $1/d^2$  as  $A = 0.0025(1/d^2) + 0.003$ ; while the coefficient  $B$  (which is related  
45 to the quadratic term of the Forchheimer equation) is a quadratic function of  $1/d$  as

46  $B = 1.14E-06(1/d)^2 - 1.26E-06(1/d)$ . The porosity ( $n$ ) can be used to reveal the effect of  
47 sorting degree and arrangement on seepage coefficient. The larger porosity leads to smaller  
48 coefficients  $A$  and  $B$  under the condition of the same particle size.

49 **Keywords:** permeable stone, mercury injection experiment, pore size, flow regime, non-  
50 Darcian flow.

## 51 1. Introduction

52 [Darcy \(1857\)](#) conducted a steady-state flow experiment in porous media and concluded  
53 that the specific discharge was proportional to the hydraulic gradient, which is the Darcy's  
54 law described as follow:

$$q = KJ \quad (1-1)$$

55 where  $q$  is the specific discharge,  $J$  is the hydraulic gradient, and  $K$  is the hydraulic  
56 conductivity. However, when the specific discharge increases above a certain threshold,  
57 deviation from Darcy's law is evident and the flow regime changes from Darcian flow regime  
58 to the so called non-Darcian flow regime ([Bear, 1972](#)), which was first observed by  
59 [Forchheimer \(1901\)](#), who proposed a widely used non-Darcian flow equation (the  
60 Forchheimer equation) as follow:

$$J = Aq + Bq^2 \quad (1-2)$$

61 where  $A$  and  $B$  are constants related to fluid properties and pore structure. The first and  
62 second terms on the right side of Eq. (1-2) roughly reflect the contributions of viscous and  
63 inertial forces (or resistance to flow), respectively.

64 From the Forchheimer equation, we can see that when the specific discharge is  
65 sufficiently small, the inertial force can be ignored, and the equation is transformed to the

66 form of Darcy's law. On the other hand, when the specific discharge is sufficiently large, the  
67 viscous force can be ignored, and the equation is transformed to the fully developed turbulent  
68 flow.

69 In addition to the polynomial function such as the Forchheimer equation, there are also  
70 several power-law functions proposed to describe the non-Darcian flow, and one of the most  
71 commonly used power-law equations is the Izbash equation ([Izbash, 1931](#)), which is written  
72 as:

$$J = aq^b \quad (1-3)$$

73 where  $a$  and  $b$  are the empirical parameters that depend on flow and materials properties, and  
74 the coefficient  $b$  is usually between 1 and 2.

75 Because of its applicability for a wide range of velocity spectrum and its sound physics,  
76 many scholars have adopted the Forchheimer equation (among many different types of  
77 equations) to explore the non-Darcian flow. Besides, the theoretical background of the  
78 Forchheimer equation has been discussed in details ([Panfilov and Fourar, 2006](#)). Numerous  
79 experimental data have confirmed the validity of the Forchheimer equation for a variety of  
80 nonlinear flow phenomena ([Geertsma, 1974](#); [Scheidegger, 1957](#); [Wright, 1968](#)). The  
81 quadratic Forchheimer law has also been revealed as a result of numerical modelling by  
82 simulating the Navier–Stokes flow in corrugated channels ([Koch and Ladd, 1996](#); [Skjetne et](#)  
83 [al., 1999](#); [Souto and Moyne, 1997](#)). To sum up, the Forchheimer equation will be selected as  
84 a representative to describe non-Darcy flow in this study.

85 Since the transition between Darcian flow and non-Darcian flow is important and  
86 difficult to quantify, different scholars have carried out experiments using a wide range of  
87 porous media, including homogeneous and heterogeneous porous media. Most of the  
88 experimental studies have focused on the influence of mean particle size on flow state

89 transition using homogeneous porous media. In fact, it was believed that the nonlinear (or  
90 non-Darcian) flow behavior in porous media was due to turbulent effect of flow in earlier  
91 studies and the Reynold number ( $Re$ ) was widely used to quantify the initiation of non-  
92 Darcian flow. [Bear \(1972\)](#) concluded that the critical  $Re$  (denoted as  $Re_c$ ) of flow states (or  
93 the  $Re$  value at which flow starts to change from Darcian flow regime to non-Darcian flow  
94 regime) is between 1 to 10. This finding was based on experimental data collected in packed  
95 sand beds ([Ergun, 1952](#); [Fancher and Lewis, 1933](#); [Lindquist, 1933](#); [Scheidegger, 1960](#)).  
96 [Schneebeli \(1955\)](#) and [Wright \(1968\)](#) experimentally measured the value of  $Re$  at the  
97 beginning of turbulence and concluded that at very high velocities, the deviation from  
98 Darcy's law is due to inertial effects followed by turbulent effects. In addition, [Dudgeon](#)  
99 [\(1966\)](#) confirmed that  $Re_c$  is about 60~150 for relatively coarse particle medium including  
100 river gravels, crushed rock particles and glass marbles with grain sizes from 16 mm to 152  
101 mm. [Dudgeon \(1966\)](#) indicated that the deviation from Darcy's law was not entirely due to  
102 turbulence, but in a large extent due to inertial forces. Besides, [Geertsma \(1974\)](#) proposed an  
103 empirical relationship among the inertial coefficient, permeability and porosity by conducting  
104 non-Darcian flow experiments in unconsolidated and consolidated sands. The laser  
105 anemometry and flow visualization studies of fluid flow in porous structures were used by  
106 [Dybbbs and Edwards \(1984\)](#), and they observed the nonlinear behavior at Reynolds numbers  
107 around 150. [Latifi et al. \(1989\)](#) found that the transition from unsteady-state laminar flow to  
108 non-Darcian flow in packed beds of spheres was between  $Re$  values of 110 and 370. [Seguin et](#)  
109 [al. \(1998\)](#) investigated the characterization of flow regimes in various porous media with  
110 electrochemical techniques and found that the end of the Darcian flow regime in packed beds  
111 of particles appeared at  $Re$  about 180. Besides, [Bu et al. \(2014\)](#) indicated that the Darcian  
112 flow in the packed beds would end at  $Re$  around 100 by using electrochemical techniques.  
113 [Sedghi-Asl et al. \(2014\)](#) found that the Darcy's law was usually not valid for rounded particle

114 sizes greater than 2.8 mm, according to the experimental results of flow in different sizes of  
115 rounded aggregates. Our previous experimental research ([Li et al., 2017](#)) indicated that when  
116 the particle size was smaller than 2.8 mm, the flow state gradually changed from pre-Darcy  
117 flow to post-Darcy flow when the specific discharge increased. When the medium particle  
118 sizes get even larger, such as 4.5 mm, 6.39 mm, 12.84 mm, and 16 mm ([Moutsopoulos et al.,  
119 2009](#)), only the post-Darcy flow exists. Based on above analysis, we can see that many  
120 previous experiments were carried out on homogeneous porous media, and the non-Darcy  
121 flow characteristics are quite different in porous media with various particle sizes.

122       Among the numerous experimental studies on this issue, it is evident that most of them  
123 focused on the effect of the mean particle size rather than the particle size distribution.  
124 Recently, a few investigators recognized the importance of particle size heterogeneity in  
125 understanding the transition of flow regimes, and have carried out a series of experiments to  
126 address the issue. For instance, [Van Lopik et al. \(2017\)](#) provided new experimental data on  
127 nonlinear flow behavior in various uniformly graded granular material for 20 samples,  
128 ranging from medium sands ( $d_{50} > 0.39$  mm) to gravel ( $d_{50} > 6.34$  mm). In addition, they  
129 investigated the nonlinear flow behavior through packed beds of 5 different types of natural  
130 sand and gravel from unconsolidated aquifers, as well as 13 different composite mixtures of  
131 uniformly graded filter sands at different grain size distributions and porosity values ([Van  
132 Lopik et al., 2019](#)). We have also discussed the effect of particle size distribution on  
133 Forchheimer flow and transition of flow regimes in a previous study ([Li et al., 2019b](#)). And  
134 our study showed that the uniformity coefficient of porous media (a term used to describe the  
135 pore size distribution) is a critical factor for determining the flow regimes besides the mean  
136 particle sizes. [Yang et al. \(2019\)](#) investigated the effects of the particle size distribution on the  
137 seepage behavior of a sand particle mixture subjected and evaluated the validity of empirical  
138 formulas of permeability and inertia factor used in engineering practice. [Shi et al. \(2020\)](#)

139 discussed the non-Darcy flow behavior of granular limestone with a wide range of porosity  
140 from 0.242 to 0.449. Based on the experimental data, [Shi et al. \(2020\)](#) proposed an empirical  
141 hydraulic conductivity-porosity relation as well as an expression of inertial coefficient.  
142 Regardless of the media investigated are homogeneous or heterogeneous, the essence of the  
143 water passing capacity of porous media is pore sizes. Thus, exploring the distribution of pores  
144 in porous media is the basis of studying flow dynamics of Darcian and non-Darcian flows.

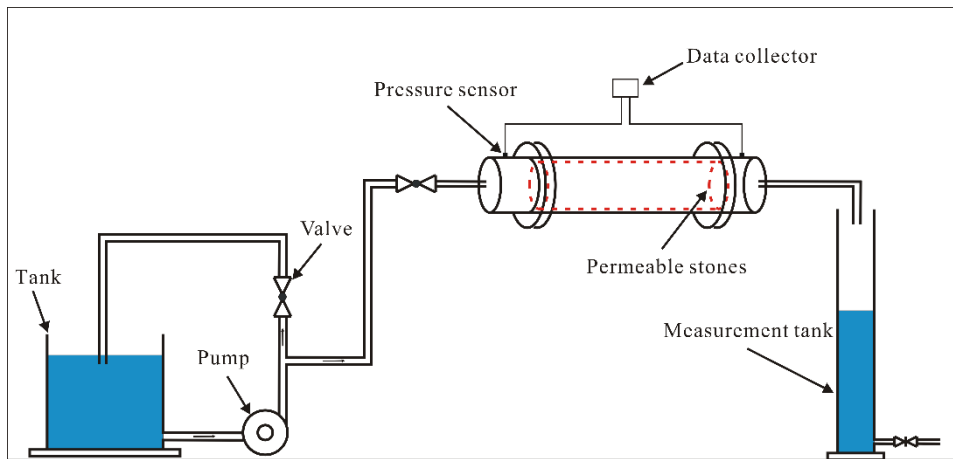
145 The purpose of this study is to provide a quantitative analysis on the effects of pore size  
146 on the transition of flow regimes between Darcian and non-Darcian flows based on a series of  
147 laboratory experiments. To meet the objectives, we have firstly carried out the seepage  
148 experiments of permeable stones with four different particle sizes. After that, we have  
149 conducted mercury injection experiments on permeable stones with four different particle  
150 sizes, and the pore size distributions with different particle sizes are obtained. Finally, the  
151 effect of pore size on the transition of flow regimes and Forchheimer coefficients are  
152 discussed based on the experimental results.

## 153 **2. Experimental methodology**

### 154 **2.1 Experimental setup and methods**

155 The experimental device is mainly composed of three parts: a water supply device, a  
156 seepage experimental device and a measuring device. The schematic diagram of the  
157 experimental apparatus is shown in Fig. 1. The water supply device consists of a tank, a  
158 centrifugal pump and a flow regulating valve. The seepage experimental device consists of a  
159 permeable stone and a plexiglass column. The measurement device monitors the real-time  
160 water temperature and pressure. The water temperature is measured using a thermometer with  
161 a precision of measurement of 0.1 °C. The water-level fluctuation is measured to calculate the  
162 flow rate by a pressure transducer (CY201, Chengdu test LLC, China) in the range of 0–20  
163 kPa with  $\pm 0.1\%$  accuracy. The measuring device consists of a cylindrical tank and a pressure

164 transducer. The sample of permeable stone is 60 mm in length with a circular cross section of  
165 51.3 mm in diameter. Two pressure transducers are set at the entrance and exit of the column  
166 to measure the pressure drop. To minimize the boundary effects, the pressure transducer is  
167 placed 30 mm away from either end of the column, and the way of pressure measurement is  
168 consistent with our previous studies ([Li et al., 2017](#); [Li et al., 2019b](#)).



169

170 Fig. 1 The schematic diagram of experimental apparatus.

## 171 2.2 Experimental Materials and Procedures

172 Four different particle sizes of permeable stones are selected to carry out the seepage  
173 experiment in this study. It is necessary to make a brief overview of the preparation process  
174 of permeable stone, which is a type of artificially made tight porous medium formed by sand  
175 grains and cementing compound. In the process of preparing permeable stone, a certain  
176 particle size of sand and cementing compound is put in a mold, and is consolidated at room  
177 temperature. Permeable stone is widely used in urban road design, sponge city construction  
178 and ecological effect research ([Guan et al., 2021](#); [Li et al., 2019a](#); [Yu et al., 2021](#)). And the  
179 most commonly used permeable base materials are large pore cement stabilized macadam,  
180 large diameter permeable asphalt mixture and so on ([Suo et al., 2021](#)). For permeable stone,  
181 there must be a certain connected pore space to maintain a certain permeability for  
182 transmitting water. However, the increase of pore space will lead to the decrease of pavement

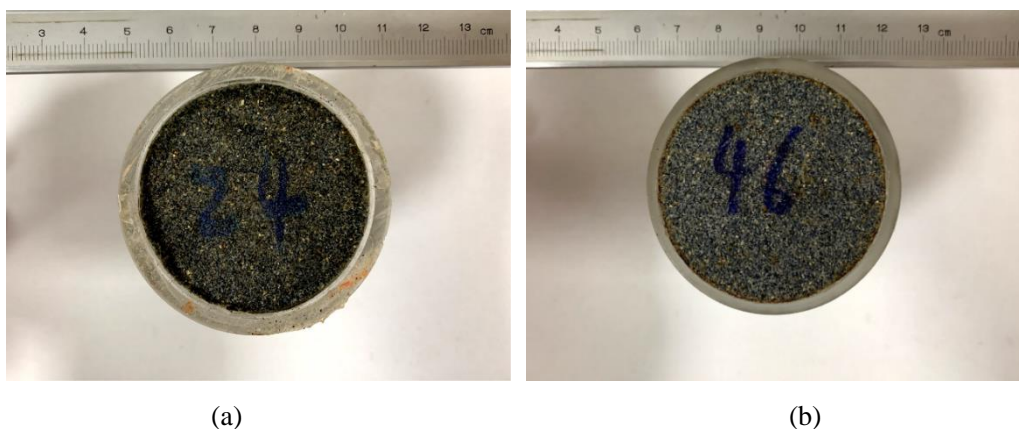


183 performance and mechanical strength (Han et al., 2016; Wang et al., 2021). Therefore, many  
184 scholars have carried out a lot of research on controlling the proper pore space of permeable  
185 stone (Alvarez et al., 2010; Prowell et al., 2002; Xie and Watson, 2004). We have carried out  
186 the seepage experiments of permeable stones with four different mesh sizes, including 24  
187 mesh size, 46 mesh size, 60 mesh size, and 80 mesh size, and the mesh size is defined as the  
188 number of mesh elements (all in square shapes) in a one inch by one inch square, thus a  
189 greater number of mesh size implies a smaller particle size. For instance, we can convert  
190 above four different mesh sizes of permeable stones into corresponding particle sizes of 0.71  
191 mm, 0.36 mm, 0.25 mm and 0.18 mm, respectively. The pore structure of permeable rock will  
192 not change in the process of the seepage experiment under room temperature, and the  
193 physical diagrams of four kinds of permeable stones with different particle sizes are shown in  
194 Fig. 2 and Fig. 3.



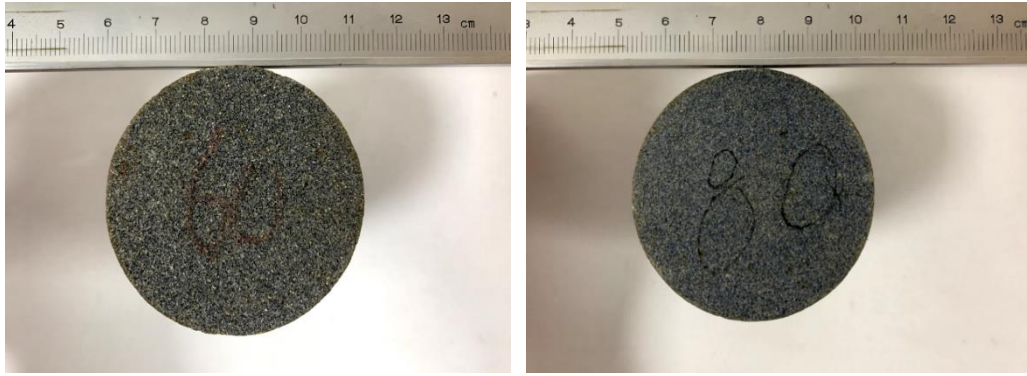
195

196 Fig. 2 Physical drawing of permeable stones with four different particle sizes.



197

198



199

200

201

202

203

204

205

206

207

208

209

210

211

212

213

214

215

216

217

218

(c)

(d)

Fig. 3 Permeable stones with different particle sizes: (a) 24 mesh size or 0.71 mm, (b) 46 mesh size or 0.36 mm, (c) 60 mesh size or 0.25 mm, and (d) 80 mesh size or 0.18 mm.

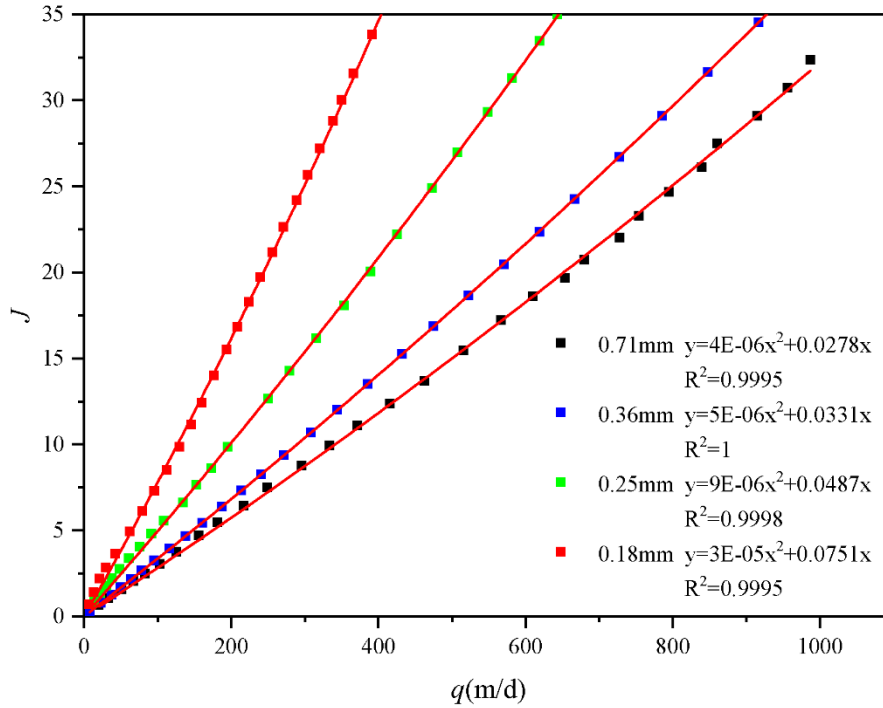
It is worth mentioning that the contact surface of the sample and the plexiglass column is sealed to prevent any preferential flow through the wall of the plexiglass column. After the permeable stone is inserted into the plexiglass column, both ends are sealed with silicone glue. The water passing through the permeable stone is then collected by a cylindrical tank. Moreover, the ratio of the internal diameter of the column to the particle size of permeable stone is greater than 12, which can eliminate any possible wall effect on the seepage according to [Beavers et al. \(1972\)](#). When carrying out the experiment, it usually takes about two hours to saturate the permeable stone. For each packed sample, more than 25 tests with different constant inlet pressures were conducted under steady-state flow condition. In addition, for each group of permeable stone, repeated tests under the same experimental condition were carried out 3-4 times to ensure the accuracy of the results.

### 3. Results and discussion

#### 3.1 Permeable stone seepage experiment

In this study, we selected permeable stone with four different particle sizes as the research objects, including 24 mesh size, 46 mesh size, 60 mesh size and 80 mesh size. The mesh size is the number of holes per inch of screen mesh and the particle size is inversely

219 proportional to the mesh size. The mean particle sizes corresponding to the four different  
220 mesh sizes are 0.71 mm, 0.36 mm, 0.25 mm, and 0.18 mm, respectively, where the mean  
221 particle size is corresponding to 50% by weight hereinafter in this study. Such a definition of  
222 mean particle size may be different from some other studies such as [Fetter \(2001\)](#) which has  
223 used 10% by weight as the mean particle size. The relationship between the specific  
224 discharge ( $q$ ) and the hydraulic gradient ( $J$ ) of permeable stones is plotted in Fig. 4. The units  
225 of specific discharge mentioned in this study are all converted to meters per day (m/d). To  
226 better compare with the actual groundwater flow, we converted the specific discharge to  
227 meters per day (m/d). Therefore, the best-fitting exercise yields Forchheimer numbers with  
228 orders of magnitudes to be about -4. In addition, the critical Forchheimer numbers proposed  
229 by [Zeng and Grigg \(2006\)](#) and [Javadi et al. \(2014\)](#) are empirical, in fact, the transition  
230 between Darcy to non-Darcy is successional over a certain range of Forchheimer numbers.  
231 The non-Darcian flow criterion applicable to different pore media is established by  
232 conducting seepage resistance experiments in homogeneous and heterogeneous porous media  
233 in our previous study ([Li et al., 2017](#); [Li et al., 2019b](#)), which is consistent with the results of  
234 [Zeng and Grigg \(2006\)](#). Generally speaking, the  $q$ - $J$  and  $q$ - $K$  curves are the most commonly  
235 used methods to analyze flow regime when conducting seepage resistance experiments in  
236 porous media. However, the nonlinear characteristics of  $q$ - $J$  curve are not obvious due to the  
237 relatively small velocity range used in the experiments. The traditional hydraulic conductivity  
238 is the ratio of the specific discharge versus the hydraulic gradient ( $q/J$ ), and it is a constant if  
239 Darcy's law is applicable, which is denoted as  $K_D$  ([Li et al., 2019b](#)). In fact, the ratio of  $q/J$  is  
240 no longer a constant for the problems discussed in this study. In a word, the  $q$ - $K$  curve can be  
241 used to observe the transition of flow state more intuitively.

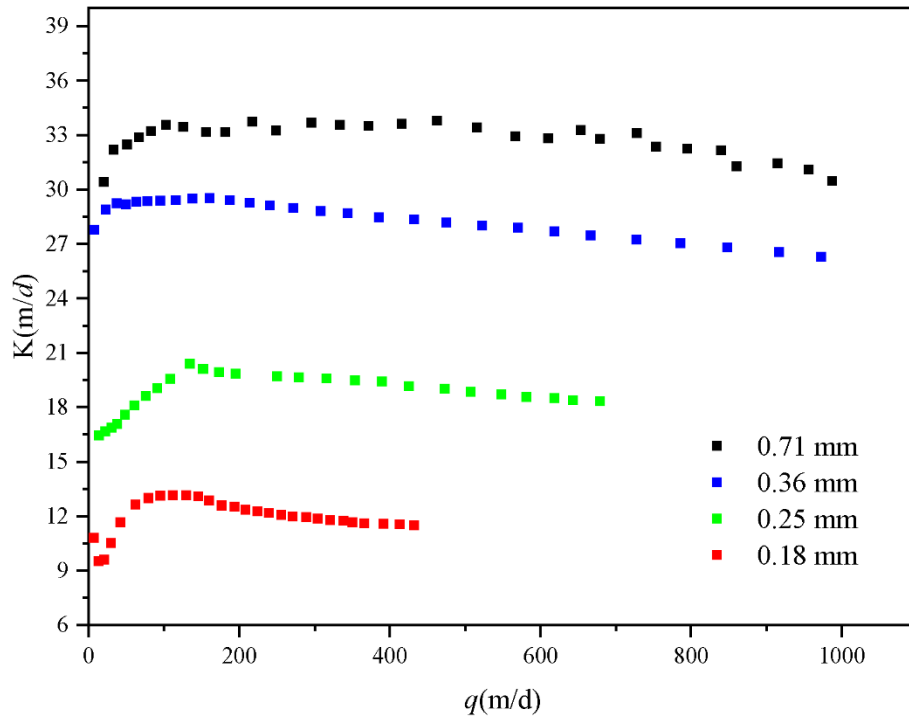


242

243 Fig. 4 Variation of  $J$  with  $q$  of four permeable stones with different particle sizes.

244

245 Fig. 4 shows that when  $q$  is somewhat the same, a larger mesh size (which means a  
 246 smaller particle size) will lead to a larger  $J$ . And the results are consistent with our previous  
 247 studies ([Huang et al., 2013](#); [Li et al., 2017](#); [Li et al., 2019b](#)). However, the nonlinear  
 248 characteristics of  $q$ - $J$  curve are not obvious due to the relatively small velocity range used in  
 249 the experiments. Nevertheless, the best-fitting results using the Forchheimer equation are  
 250 satisfactory. To analyze the influence of pore size on seepage flow regimes, we have obtained  
 251 the relationship between  $q$  and the “pseudo” hydraulic conductivity ( $K$ ) (which is computed  
 252 using  $q/J$ ) of four permeable stones with different particle sizes, as shown in Fig. 5. We  
 253 should point out that the “pseudo” hydraulic conductivity term discussed here for non-  
 254 Darcian flow is usually not a constant, thus it is different from the hydraulic conductivity  
 255 term used in Darcy’s law, which is a constant. It is obvious that the hydraulic conductivity is  
 256 not a constant with the increase of specific discharge, so it is called the “pseudo” hydraulic  
 conductivity ([Li et al., 2019b](#)).



257

258 Fig. 5 Variation of  $K$  with  $q$  of four permeable stones with different particle sizes.

259 We can divide the  $q$ - $K$  curve into two segments: for the first segment,  $K$  increases with  
 260 the increase of  $q$ , which is denoted as the pre-Darcian flow. For the second segment, after  $q$   
 261 increases to a certain value,  $K$  begins to decrease with  $q$ , which is called the post-Darcian

262 flow. In fact, [Izbash \(1931\)](#) presented the equation as  $q = M \left( \frac{dH}{dx} \right)^m = Mi^m$ , where  $M$  and  $m$

263 are the coefficients determined by fluid flow and properties of porous media. When  $m=1$ , the

264 Izbash equation reduces to Darcy law, when  $m>1$ , the Izbash equation corresponds to the pre-

265 Darcy flow and when  $m<1$ , the Izbash equation refers to the post-Darcy flow ([Dejam et al.,](#)

266 [2017](#); [Soni et al., 1978](#)). Besides, [Dejam et al. \(2017\)](#) carried out a more detailed study on

267 issues related to the pre-Darcy and post-Darcy flows. And the influence of pre-Darcy flow on

268 the pressure diffusion for homogenous porous media is studied in terms of the nonlinear

269 exponent and the threshold pressure gradient. When the hydraulic gradient is small (and  $q$  is

270 small as well), a great portion of water is bounded (or becomes immobile) on the surface of

271 solids due to the solid-liquid interfacial force, and only a small fraction of the water is mobile

272 and free to flow through the pores. In addition, another justification for the pre-Darcy  
273 behavior may be due to an effect of a stream potential which generates small countercurrents  
274 along pore walls in a direction opposite that of the main flow ([Bear, 1972](#); [Scheidegger, 2020](#)).  
275 And [Swartzendruber \(1962b\)](#) stated that the surface forces arose in a solid-fluid interface due  
276 to strong negative charges on clay particle surfaces and the dipolar nature of water molecules  
277 caused a pressure gradient response to be nonlinear and led to the pre-Darcy flow  
278 ([Swartzendruber, 1962a](#)). As the hydraulic gradient increases (and  $q$  increases as well), the  
279 initial threshold for mobilizing the previously immobile water near the solid-liquid surface is  
280 overcome and more water participates in the flow. For this reason, the "pseudo" hydraulic  
281 conductivity increases with the increase of hydraulic gradient and the specific discharge in  
282 the first segment. When the specific discharge increases to the critical specific discharge ( $q_c$ ),  
283 the "pseudo" hydraulic conductivity is maximized. According to  $K = \frac{q}{Aq + Bq^2} = \frac{1}{A + Bq}$   
284 based on Eq. (1-2), we can find that the "pseudo" hydraulic conductivity begins to decrease  
285 as the specific discharge continues to increase. Besides, the critical specific discharge  
286 corresponding to the transition of flow regimes (from pre-Darcian to post-Darcian) increases  
287 with the increase of particle sizes (or decrease of mesh sizes).

### 288 **3.2 Mercury injection experiment**

289 The particle size, different grain size distributions and degree of sorting are the main  
290 factors that determine the size and shape of pores. And the shape of the pores determines the  
291 tortuosity and distribution of flow paths, which are related to viscous and inertial flow  
292 resistances. It is generally accepted in previous studies that the pore sizes of porous media  
293 have an impact on the seepage law ([Maalal et al., 2021](#); [Zhou et al., 2019](#)). However, the  
294 structure of natural porous media is very complex, and it is difficult to quantify the effects of  
295 the arrangement of particles on the seepage law. The characteristics of pore size distribution

296 contains critical information for quantifying the flow regimes. The mercury intrusion  
297 porosimetry and the nitrogen adsorption isotherm are two commonly used methods to  
298 characterize the pore sizes and their distribution ([Rijfkogel et al., 2019](#)). Besides, other  
299 techniques can also be used to derive the pore size distribution, such as small-angle neutron  
300 and X-ray scattering measurements, CT images and nuclear magnetic resonance ([Anovitz and](#)  
301 [Cole, 2015](#); [Hall et al., 1986](#); [Kate and Gokhale, 2006](#); [Lindquist et al., 2000](#)). In this study  
302 we will use the mercury injection experiment to measure the pore size distribution of the four  
303 permeable stones with different particle sizes and use the information to describe the flow  
304 regimes.

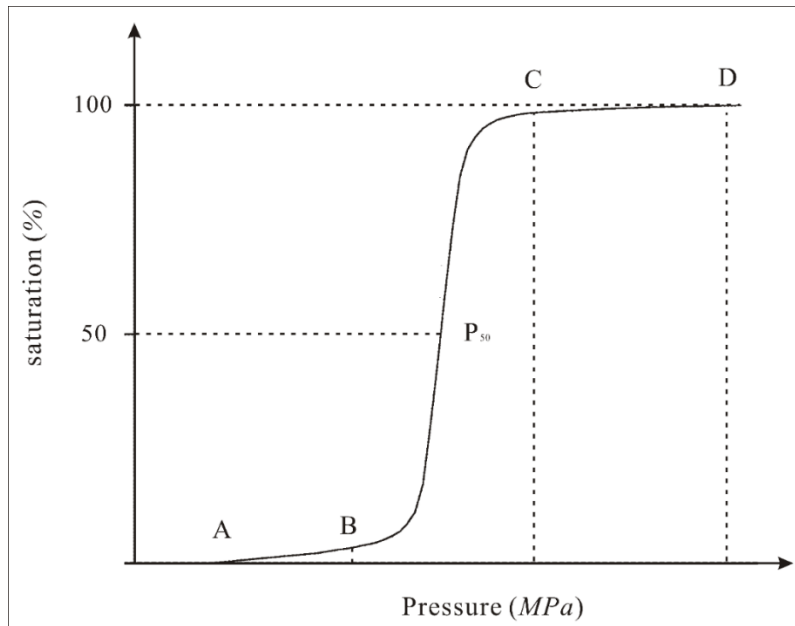
305 To quantitatively study the pore size and pore throat distribution, we need to envisage a  
306 physically based conceptual model to describe the pore structures of permeable stones. The  
307 commonly used model is the so-called capillary model ([Pittman, 1992](#); [Rezaee et al., 2012](#);  
308 [Schmitt et al., 2013](#)), which approximates the connected pores as many paralleled capillaries.  
309 And the capillary forces are generated at the phase interface due to the surface tension  
310 between the solid and liquid phases when liquid flows in a capillary. The capillary force is  
311 directed toward the concave liquid level, and is shown as ([Washburn, 1921](#)):

$$P_c = \frac{2\sigma \cos \theta}{r} \quad (3-1)$$

312 where  $P_c$  is the capillary force,  $\sigma$  is the solid-liquid interfacial tension,  $\theta$  is the wet angle  
313 between the liquid and the solid surface, and  $r$  is the radius of curvature in capillary.

314 Since mercury is a nonwetting phase to solids, so to get mercury into the pores of the  
315 permeable stone, an external force (or displacement pressure) must be applied to overcome  
316 the capillary force. When a greater pressure is applied, mercury can enter smaller pores.  
317 When a certain pressure is applied, the injection pressure is equivalent to the capillary  
318 pressure in the corresponding pore. Then we can calculate the corresponding capillary radius

319 according to Eq. (3-1), and the volume of mercury injected is the pore volume.



320

321 Fig. 6 Schematic diagram of pressure changes with saturation: the initial stage (A-B), the  
322 intermediate mercury entry stage (B-C), and the end stage (C-D).

323 By continuously increasing the injection pressure, one can obtain the curve of injection  
324 pressure and the volume of injected mercury, from which one can also obtain the pore-throat  
325 distribution curve and capillary pressure curve. According to the amount of mercury injected  
326 at different injection pressures, the relation between the injection pressure and the injection  
327 saturation is shown in Fig. 6.

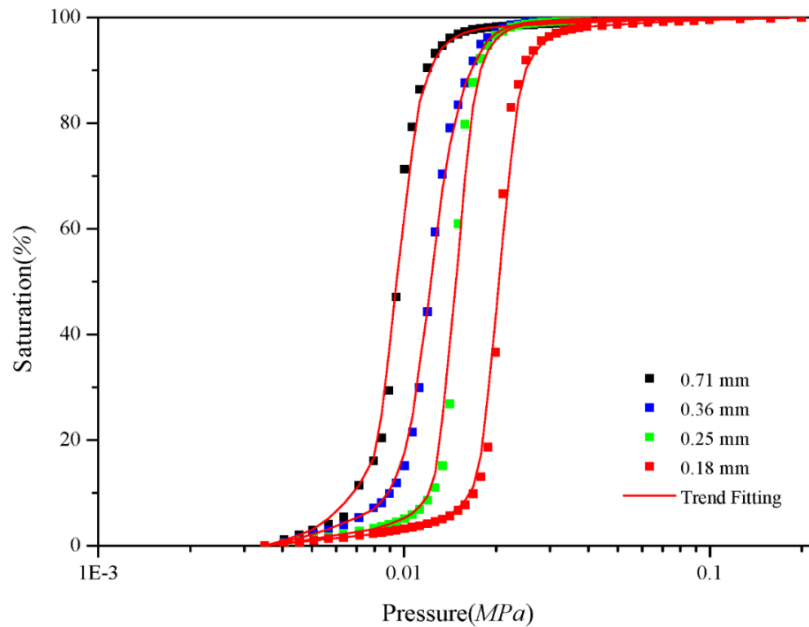
328 Fig. 6 shows that the mercury injection curve can be divided into three stages. Firstly,  
329 during the initial stage (A-B) which has a very mild slope, the intake pressure is very small  
330 and the intake saturation is also very low. With the increasing of the injection pressure, the  
331 intake saturation slowly increases. Secondly, during the intermediate mercury entry stage (B-  
332 C) which has a steep slope, a small pressure change will lead to a significant saturation  
333 change. This means that the pores are relatively uniform and the differences in pore sizes are  
334 small. It is well known that for mercury injection experiments, as injection pressure increases,  
335 the injection saturation will gradually increase and eventually all the pores will be filled with



336 mercury. As can be seen from Fig. 7, with the continuous injection of mercury, the pressure of  
337 permeable stones with different particle sizes varies with saturation, which is reflected in the  
338 different pressure  $P_B$  and  $P_C$  at different stages. However, the reason for the different pressure  
339 is the difference of pore size distribution in the permeable stones. Therefore, the pressure  
340 ratio of B and C ( $P_C/P_B$ ) can be used as one of the criteria to characterize the heterogeneity of  
341 pore size in porous media. Besides, when the saturation reaches 50%, the corresponding  
342 pressure value ( $P_{50}$ ) reflects the characteristics of the mean pore size, and a larger  $P_{50}$  leads to  
343 a larger mean pore size. Finally, during the end stage (C-D) which has a very mild slope as  
344 well, the amount of mercury will not increase considerably when the injection pressure  
345 increases. This indicates that nearly all the pores are essentially filled with mercury, and the  
346 mercury injection experiment is completed. After completing the mercury injection  
347 experiments, we have obtained the mercury injection curves of four permeable stones with  
348 different particle sizes, as shown in Fig. 7.

349 We can make a number of interesting observations based on Fig. 7. Firstly, the pressure  
350 at the starting point (when the saturation begins to increase), denoted as  $P_A$ , increases as the  
351 mean particle size decreases. This means that the maximum pore size in permeable stone  
352 decreases with the decrease of the mean particle sizes. Secondly, the mercury injection curves  
353 of four permeable stones all include steep intermediate stages, indicating that the pore size  
354 distributions are all relatively uniform. And the corresponding pressure values at points B and  
355 C increase as the mean particle sizes decreases. Moreover, the pressure ratios corresponding  
356 to points B and C ( $P_C/P_B$ ) also decrease with the decrease of particle sizes, suggesting even  
357 more uniform pore size distributions with decreasing particle sizes. Thirdly, the intermediate  
358 mercury entry stages gradually shift to the right with the decrease of particle sizes. When the  
359 saturation reaches 50%, the corresponding pressure (the median pressure) decreases with the  
360 increase of the mean particle sizes. Fourthly, the mercury injection curves of these four

361 permeable stones with different particle sizes all approach 100% saturation with very mild  
 362 slopes, indicating that there are few small pores in the permeable stones. We have extracted  
 363 the key pressure characteristic values of mercury injection experiment of Fig. 7, and listed the  
 364 results in Table 1.



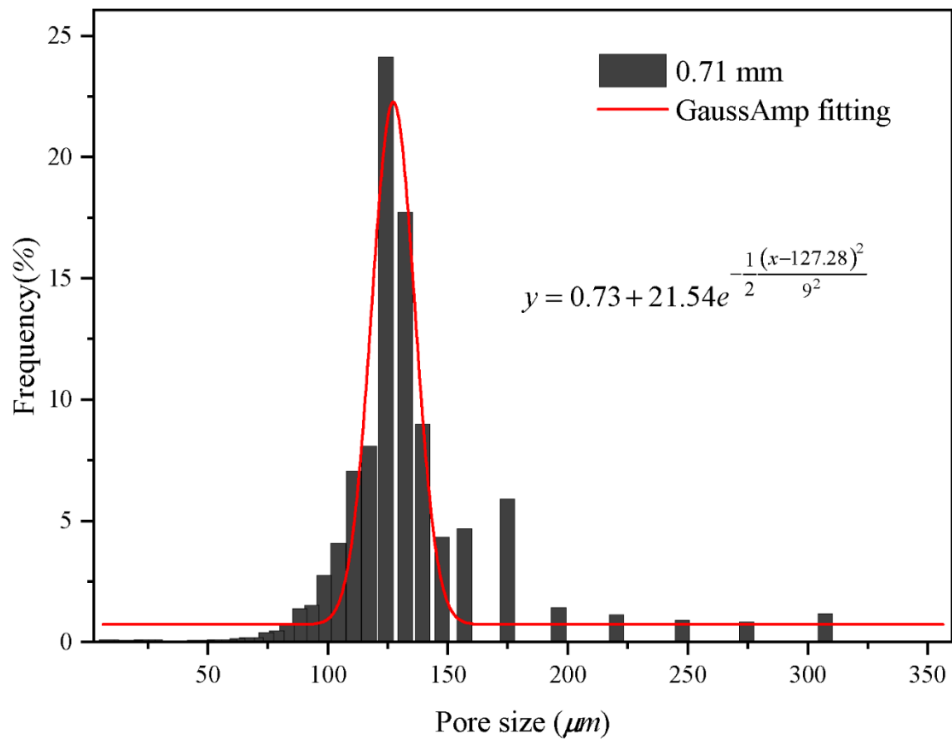
365  
 366 Fig. 7 Variation of pressure with saturation of four permeable stones with different particle  
 367 sizes.

368 Table 1. Pressure characteristic values of four permeable stones with different particle sizes.

Mesh size	$P_A(MPa)$	$P_B(MPa)$	$P_C(MPa)$	$P_{50}(MPa)$	$P_C/P_B$
24	0.0041	0.0064	0.0133	0.0094	2.0987
46	0.0045	0.0071	0.0188	0.0119	2.6374
60	0.0051	0.0112	0.0211	0.0150	1.8764
80	0.0057	0.0158	0.0281	0.0211	1.7758

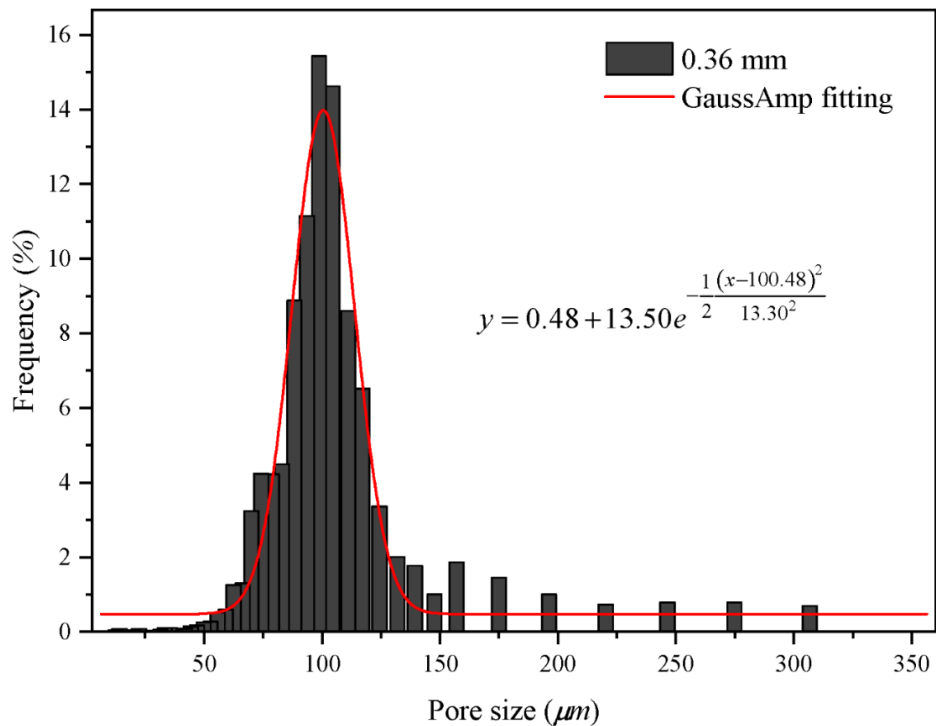
369 To observe the pore size distributions of the four permeable stones with different particle

370 sizes in more details, we can calculate the percentages of different pore sizes in permeable  
 371 stones according to the mercury injection curves, as shown in Figs. 8-11.



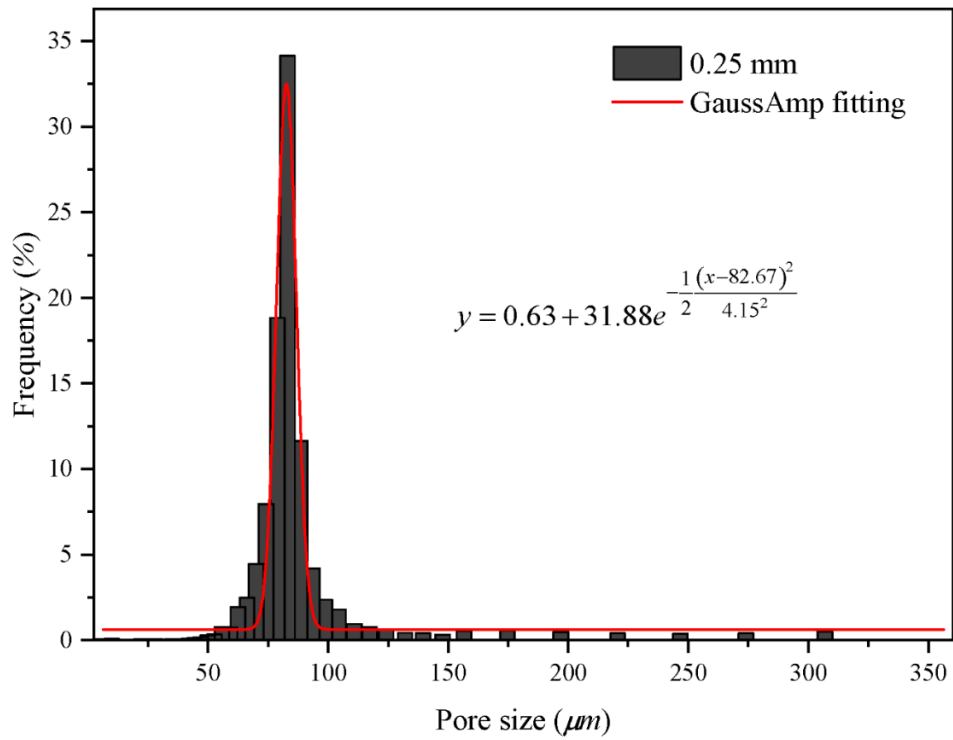
372

373 Fig. 8 Histogram of pore size distribution of permeable stone with diameter of 0.71 mm.



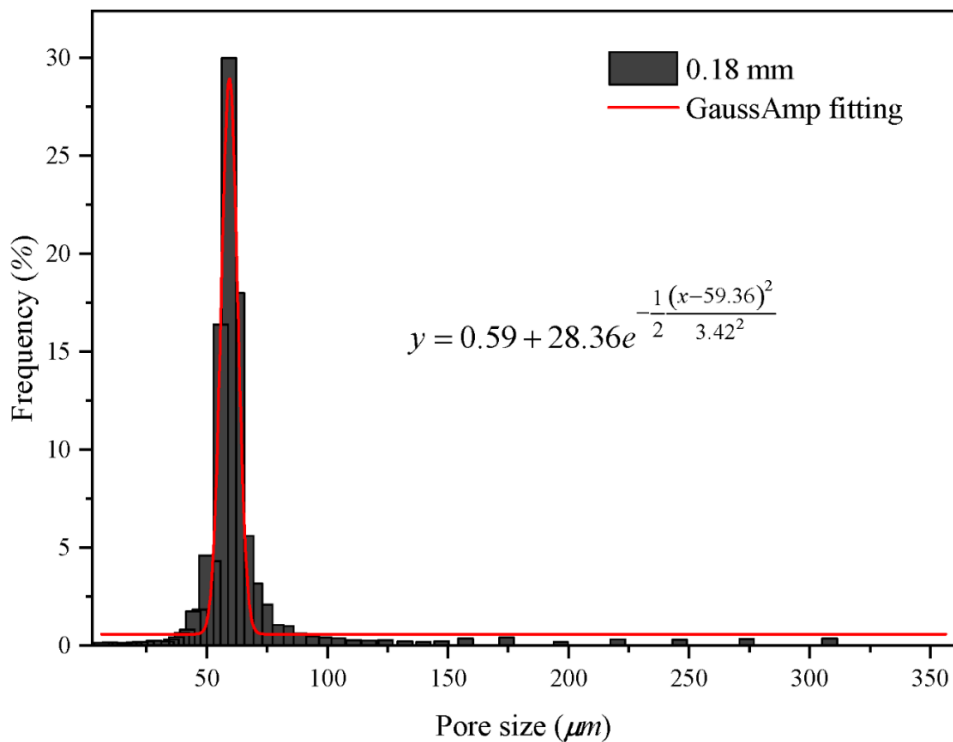
374

375 Fig. 9 Histogram of pore size distribution of permeable stone with diameter of 0.36 mm.



376

377 Fig. 10 Histogram of pore size distribution of permeable stone with diameter of 0.25 mm.



378

379 Fig. 11 Histogram of pore size distribution of permeable stone with diameter of 0.18 mm.

380 From Fig. 8 to Fig. 11 we can find that the pore sizes of the four permeable stones are

381 uniform and fall within narrow ranges. The pore size distributions of four different particle  
382 sizes show a skewed normal distribution. Besides, the pore maximum proportion (the peak of  
383 the curve, see Figs. 8-11) of permeable stones with different particle sizes are different, which  
384 are 124  $\mu\text{m}$ , 99  $\mu\text{m}$ , 83  $\mu\text{m}$  and 59  $\mu\text{m}$ , respectively. The Gaussian function is widely used to  
385 characterize the pore system and classify the petrophysical rock ([Harlan et al., 1995](#); [Jeon et](#)  
386 [al., 2014](#); [Xu and Torres-Verdín, 2013](#)), and the general form of the Gauss function is shown  
387 below:

$$y = y_0 + He^{-\frac{(x-x_c)^2}{2w^2}} \quad (3-2)$$

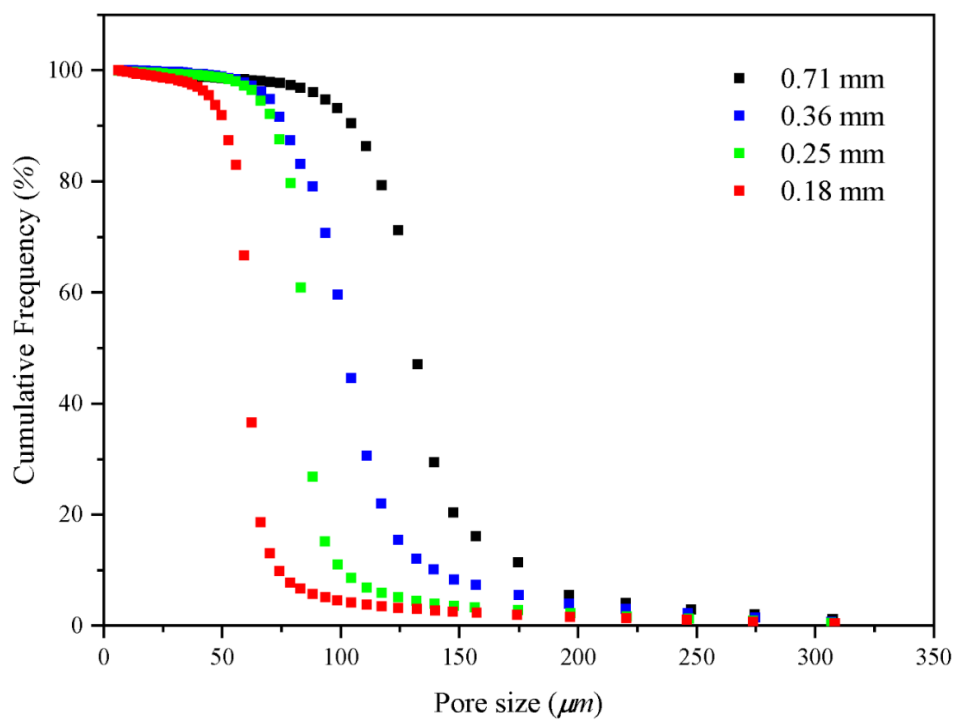
388 where  $H$  is the height of the peak of the mercury injection curve,  $x_c$  is the abscissa  
389 corresponding to the peak of the curve (the pore size),  $w$  is the standard variance, which  
390 represents the width of the curve. To characterize the distribution of pore structure of four  
391 different permeable stones, we best-fit the Gaussian curve of the pore distribution of four  
392 permeable stones with different particle sizes, and the best-fitted parameters are shown in  
393 Table 2. We can make several interesting observations from Table 2. Firstly, the expected  
394 value ( $x_c$ ) decreases with decreasing particle sizes of permeable stone, and the  $x_c$  values of  
395 different permeable stones are almost the same. Secondly, the standard variance ( $w$ )  
396 corresponding to the permeable stone of 0.18 mm is the smallest, indicating that the pore size  
397 distribution is more concentrated (or relatively homogeneous). For comparison, the pore size  
398 distribution of 0.36 mm permeable stone is the widest with the greatest variance. Finally,  
399 different values of  $H$  represent different proportions of pore sizes, among which the highest  
400 proportion can reach 34.04%. It will be desirable to establish a correlation between the  
401 parameters used in the pore-size distribution of Eq. (3-2) with the two Forchheimer  
402 coefficients  $A$  and  $B$ . This objective may be achieved using high-resolution pore-scale fluid  
403 mechanics simulations, which are out of the scope of this study. Further research is needed to

404 address this issue in the future.

405 Table 2. Gaussian function characteristic values of four permeable stones with different  
 406 particle sizes.

Mesh size	particle size (mm)	$y_0$	$H$	$x_c$	$w$
24	0.71	0.73	21.54	127.28	9.00
46	0.36	0.48	13.49	100.48	13.30
60	0.25	0.63	31.88	82.67	4.15
80	0.18	0.59	28.36	59.36	3.42

407 The pore size distributions fall within ever narrower ranges with mesh sizes become  
 408 larger. Moreover, the cumulative percentage frequency curves of the pore size distributions  
 409 with different particle sizes are exhibited in Fig. 12 and the results are shown in Table 3.



410

411

Fig. 12. The cumulative frequency curve of pore size distribution.

412 Fig. 12 shows that  $R_{50}$  (the pore size corresponding to the median pressure  $P_{50}$ ) increases  
 413 with the increase of permeable stone particle size, and the mean pore diameter ( $R_m$ ) also  
 414 increases. In general, the pore size corresponding to the median pressure (denoted as  $R_{50}$ )  
 415 may be slightly different than the mean pore diameter ( $R_m$ ) which has been defined in  
 416 different ways by various investigators when analyzing the pore size distributions ([Hea and](#)  
 417 [Zhangb, 2015](#); [Zhen-Hua et al., 2007](#); [Zhihong et al., 2000](#)). As  $R_{50}$  is easily identifiable in  
 418 the mercury injection experiments, it is used in this study as a representative of the mean pore  
 419 diameter ( $R_m$ ) of the permeable stone. Besides, the seepage law of permeable stone is closely  
 420 related to the pore size, and the smaller average pore size will result in a larger hydraulic  
 421 gradient under the condition of the same specific discharge (see Fig. 4). The pore size  
 422 characteristic values with different particle sizes are listed in Table 3. We find that the  
 423 porosity decreases as the particle size increases while the mean pore diameter increases. And  
 424 the mean pore size can reflect the influence of particle diameter, sorting degree and  
 425 arrangement mode of porous medium on seepage parameters.

426 Table 3. Pore size characteristic values of four permeable stones with different particle sizes.

Mesh size	Mean particle size (mm)	Porosity (%)	$R_m$ ( $\mu\text{m}$ )	$R_{50}$ ( $\mu\text{m}$ )
24	0.71	32.35	131.31	131.34
46	0.36	36.69	102.56	103.42
60	0.25	40.82	84.73	85.09
80	0.18	42.88	60.97	61.12

427 Note:  $R_m$  is the mean pore diameter,  $R_{50}$  is the pore diameter corresponding to the median  
 428 pressure  $P_{50}$ .

429 **3.3 Analysis of influencing factors of Forchheimer equation coefficients**

430 **3.3.1 Influence of particle size on equation coefficient**

431 The analysis of non-Darcy coefficient has always been of interest to many researchers  
 432 working in different disciplines of porous media flow ([Moutsopoulos et al., 2009](#); [Sedghi-Asl](#)  
 433 [et al., 2014](#); [Shi et al., 2020](#)). Various studies have suggested expressions for Forchheimer  
 434 coefficients, different scholars obtained numerous datasets through different experiments and  
 435 simulation methods to quadratic best-fitting the specific discharge-hydraulic gradient curves.  
 436 And the coefficients of different fitting equations are shown in the following Table 4.

437 **Table 4.** The Forchheimer coefficients of empirical relations.

Equations	Coefficient A (s/m)	Coefficient B (s <sup>2</sup> /m <sup>2</sup> )
<a href="#">Ward (1964)</a>	$A = \frac{360}{gd^2}$	$B = \frac{10.44}{gd}$
<a href="#">Blick (1966)</a>	$A = \frac{32}{gnd^2}$	$B = \frac{C_D}{2gn^2d}$
<a href="#">Ergun (1952)</a>	$A = \frac{150(1-n)^2}{gn^3d^2}$	$B = \frac{1.75(1-n)}{gn^3d}$
<a href="#">Macdonald et al. (1979)</a>	$A = \frac{180(1-n)^2}{gn^{3.6}d^2}$	$B = \frac{1.8(1-n)}{gn^{3.6}d}$
<a href="#">Kovács (1981)</a>	$A = \frac{144(1-n)^2}{gn^3d^2}$	$B = \frac{2.4(1-n)}{gn^3d}$
<a href="#">Kadlec and Knight (1996)</a>	$A = \frac{255(1-n)^2}{gn^{3.7}d^2}$	$B = \frac{2(1-n)}{gn^3d}$
<a href="#">Irmay (1964)</a>	$A = \frac{180(1-n)^2}{gn^3d^2}$	$B = \frac{0.6(1-n)}{gn^3d}$

438 [Sidiropoulou et al. \(2007\)](#) focused on the determination of the Forchheimer coefficients  
 439 for non-Darcian flow in porous media and evaluated the original theoretical equations above  
 440 and the validity of these equations was checked using existing experimental data. In addition,  
 441 the Root Mean Square Error (RMSE) was used as a criterion to quantitatively evaluate the



442 coefficients, and the RMSE was defined as  $RMES = \sqrt{\frac{\sum_{i=1}^N (x_i - y_i)^2}{N}}$ , where  $x_i$  were the  
 443 experimental values of Forchheimer coefficients,  $y_i$  were the values computed by different  
 444 equations above, and  $N$  was the total number of experimental points ([Moutsopoulos et al.,](#)  
 445 [2009](#)). The different forms of Forchheimer coefficients described above are based on different  
 446 assumptions and simplifications of pore structure. Consequently, these series of coefficients  
 447 are applicable under specific conditions with different degrees of accuracy.

448 According to Eq. (1-2), the hydraulic gradient ( $J$ ) is composed of a viscous force-related  
 449 component ( $J_n$ ) and an inertia force-related component ( $J_r$ ), and for specific derivation, please  
 450 refer to previous studies ([Huang, 2012](#)):

$$J_n = Aq = \frac{\alpha\mu}{\rho g} \frac{1}{d^2} q \quad J_r = \frac{\beta}{g} \frac{1}{d} q^2 \quad (3-3)$$

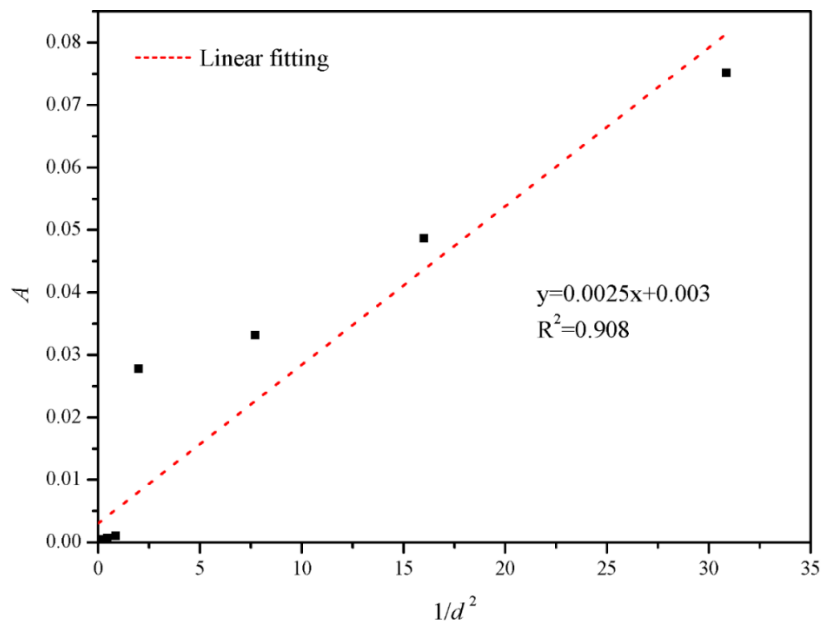
451 We can see from Eq. (3-3) that the  $J_n$  is inversely proportional to the square of the particle  
 452 size, and the  $J_r$  is inversely proportional to the particle size when the specific discharge  
 453 remains the same. Both  $J_n$  and  $J_r$  are closely related to specific surface area and sizes of pores.  
 454 Therefore, the particle size is an important factor affecting the Forchheimer coefficient,  
 455 [Huang et al. \(2013\)](#) carried out the experimental investigation on water flow in four columns  
 456 with cubic arrays of acrylic balls in diameter 3 mm, 5 mm, 8 mm and 10 mm, where all the  
 457 acrylic balls are arranged in regular cubes. Accordingly, the coefficients  $A$  and  $B$  can be  
 458 written as follows:

$$A = \frac{\alpha\mu}{\rho g} \frac{1}{d^2} \quad B = \frac{\beta}{g} \frac{1}{d} \quad (3-4)$$

459 where  $\alpha$  and  $\beta$  are constants related to the shape, sorting, and arrangement of the particles,  
 460 and the specific derivation process is detailed in the previous study ([Huang, 2012](#)). The

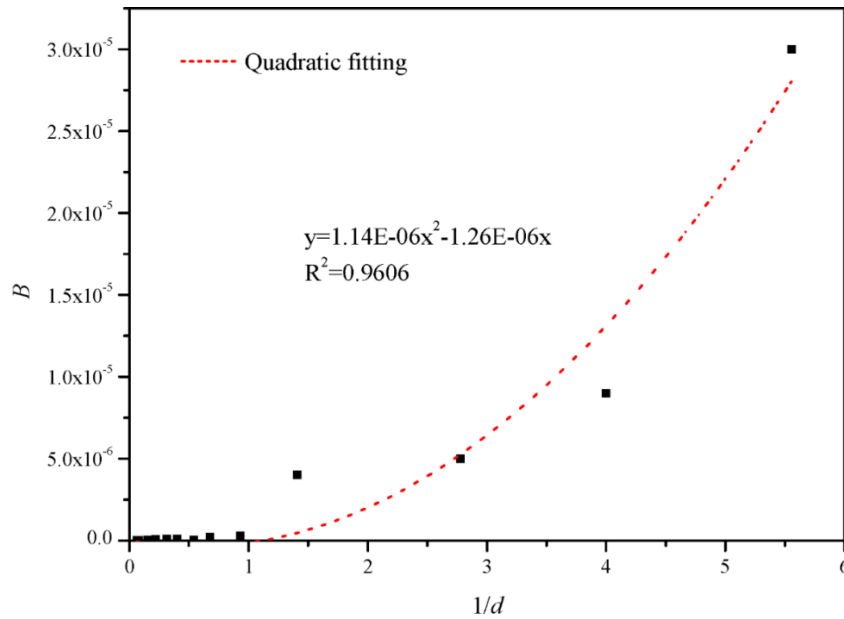
461 experimental results showed that the coefficient  $A$  was inversely proportional to the particle  
462 diameter square ( $d^2$ ) and coefficient  $B$  was inversely proportional to the particle size ( $d$ )  
463 ([Huang et al., 2013](#)).

464 The uniform diameter cubic arrangement of porous media mentioned above is a rather  
465 ideal medium. The shape and arrangement of particles of natural pore aquifers are usually  
466 irregular. Therefore, the above-mentioned linear correlations between  $A$  and  $1/d^2$ , and  
467 between  $B$  and  $1/d$  should be examined specifically. For this purpose, we collect the  
468 experimental data of homogeneous porous media, including the previous research results and  
469 the results of other scholars. Among them, samples P1-P4 are the permeable stones selected  
470 in this study, samples L1-L5 are from previous studies ([Li et al., 2017](#)), and the experimental  
471 data of samples M1-M4 are from [Moutsopoulos et al. \(2009\)](#). The fitting coefficients are  
472 shown in Table 5. Furthermore, we can identify nice correlations between the Forchheimer  
473 coefficient  $A$  and  $1/d^2$  and between the Forchheimer coefficient  $B$  and  $1/d$ , which are shown  
474 in Fig. 13 and Fig. 14, respectively.



475

476 Fig. 13. Variation of  $A$  with  $1/d^2$  of different homogeneous particle sizes.



477

478

Fig. 14. Variation of  $B$  with  $1/d$  of different homogeneous particle sizes.

479

480

481

482

483

484

485

486

487

488

489

490

491

We can see from Fig. 13 that the coefficient  $A$  is linearly related to  $1/d^2$  and the relationship between coefficient  $A$  and is given as  $A = 0.0025(1/d^2) + 0.003$ . And the relationship between coefficient  $B$  and  $1/d$  is completely different from the linear correlation as reported before. Fig. 14 shows that the coefficient  $B$  is quadratic related to  $1/d$  and the relationship between coefficient  $B$  and  $1/d$  is given as  $B = 1.14E-06(1/d)^2 - 1.26E-06(1/d)$ . That is to say, the relationship between coefficient  $A$  and  $1/d^2$  is consistent with the law of simple cubic arrangement porous media, but the relationship between coefficient  $B$  and  $1/d$  is not consistent with the law of simple cubic arrangement porous media. The structure of porous medium arranged in cubes is different from the permeable stone. The porosity of the porous media with spheres arranged in cubic is close to 0.48, independent of the diameter of spheres. While the particle shape, arrangement and tightness of permeable stone are different, and the porosity of permeable stone with different particle size is also different (see Table 3).

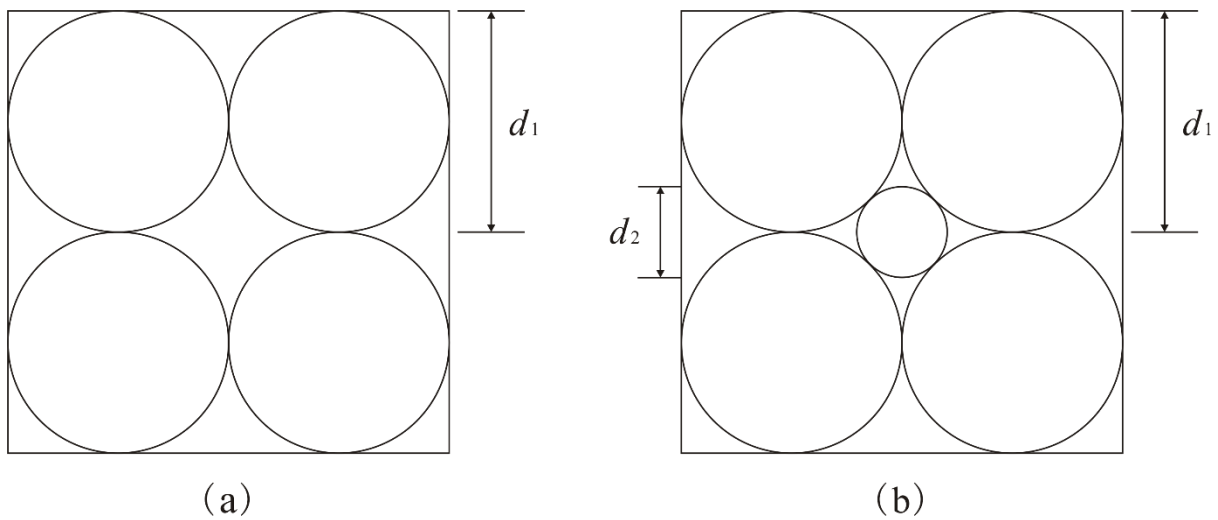
Table 5. Experimental fitting coefficient of different homogeneous particle sizes.

Sample	Particle size (mm)	Fitting equation	A	B	The correlation
P1	0.18	$y=0.0751x+3E-05x^2$	0.0751	3E-05	0.9995
P2	0.25	$y=0.0487x+9E-06x^2$	0.0487	9E-06	0.9998
P3	0.36	$y=0.0331x+5E-06x^2$	0.0331	5E-06	1
P4	0.71	$y=0.0278x+4E-06x^2$	0.0278	4E-06	0.9995
L1	1.075	$y=0.001x+3E-07x^2$	0.001	3E-07	0.9999
L2	1.475	$y=0.0007x+2E-07x^2$	0.0007	2E-07	0.9998
L3	1.85	$y=0.0005x+5E-08x^2$	0.0005	5E-08	0.9998
L4	2.5	$y=0.0005x+9E-08x^2$	0.0005	9E-08	0.9997
L5	3.17	$y=0.0004x+1E-07x^2$	0.0004	1E-07	0.9998
M1	4.5	$y=3E-05x+7E-08x^2$	3E-05	7E-08	0.9913
M2	6.39	$y=3E-05x+3E-08x^2$	3E-05	3E-08	0.9984
M3	12.84	$y=1E-05x+2E-08x^2$	1E-05	2E-08	0.9977
M4	16	$y=1E-05x+2E-08x^2$	1E-05	2E-08	0.998

### 492 3.3.2 Influence of porosity on equation coefficient

493 In above sections, we have analyzed the influence of particle sizes on seepage  
494 coefficient. Furthermore, the pore size and pore specific surface area are also related to the  
495 arrangement and sorting degree of particles, that is, to the porosity of porous media. To  
496 explore the effect of sorting degree on seepage coefficient, we draw a schematic diagram of  
497 different sorting degree of particles, as shown in Fig. 15. The degree of particle sorting is one

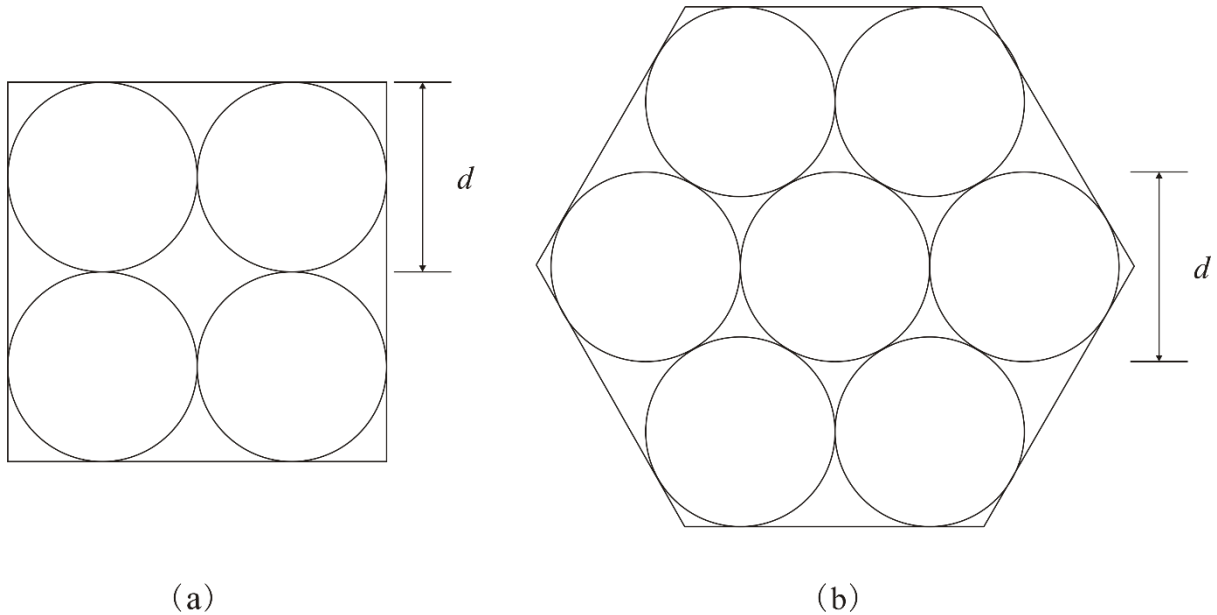
498 of the important factors affecting the pore size. In porous media with a poor sorting degree,  
 499 the pore size is usually determined by the diameter of the smallest particle. We can see from  
 500 Fig. 15 that the pores between the larger particles are filled by smaller particles, resulting in  
 501 even smaller pores. In addition, the poorer sorting degree of particles leads to the larger pore  
 502 specific surface area and stronger viscous force of flow, which can lead to a larger coefficient  
 503 A.



504 (a) (b)  
 505 Fig. 15. The schematic diagram of different particle sorting with cube arrangement.

506 Furthermore, we have also provided the schematic diagrams of spherical particles with  
 507 equal size in two simple arrangements, namely cube arrangement and hexahedron  
 508 arrangement, as shown in Fig. 16. And the cube arrangement is the less compact arrangement  
 509 with a pore diameter of  $0.414d$ , while the hexahedron arrangement is the more compact  
 510 arrangement with a pore diameter of  $0.155d$ . The characteristic value of pore structure in  
 511 different arrangement with the same particle size are shown in Table 6. We can see that  
 512 different arrangement modes will substantially affect the pore specific surface area and pore  
 513 size of porous media. The more compactly packed particles lead to the larger pore specific  
 514 surface area and stronger viscous force. Meanwhile, the smaller pore diameter is associated  
 515 with stronger effect of viscous force and inertia force. In summary, the better sorting degree

516 of particles leads to the weaker viscous and inertial forces, then the coefficients  $A$  and  $B$  will  
 517 be smaller. As the better sorting degree and the less compact (or looser) arrangement particles  
 518 mean the larger porosity, so we can conclude that the larger porosity leads to the smaller  
 519 coefficients  $A$  and  $B$  under the condition of the same particle size.

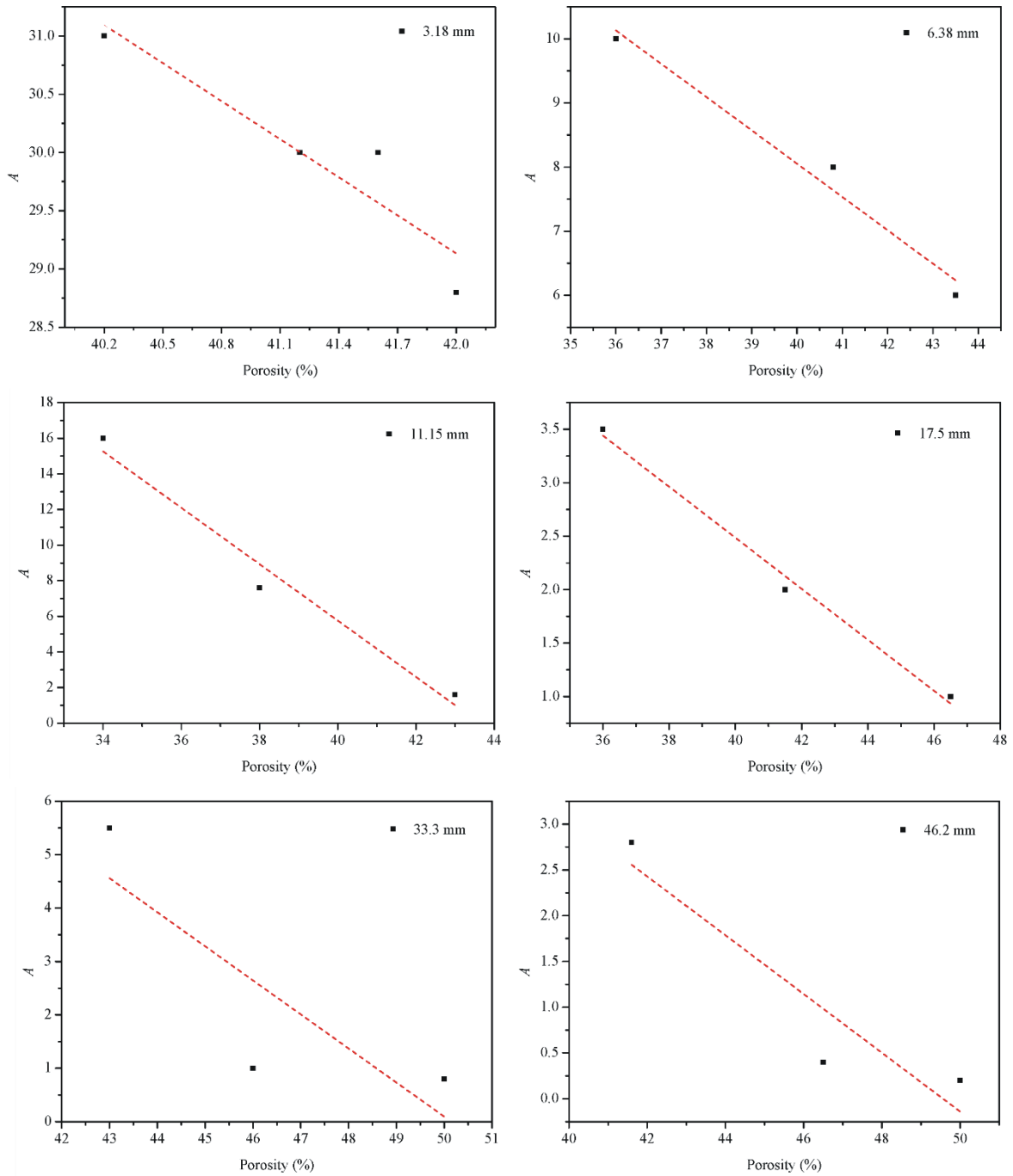


520 (a) (b)  
 521 Fig. 16. The schematic diagram of cube and hexahedron arrangement with the same particle  
 522 size.

523 Table 6. Characteristic value of pore structure in different arrangement with the same particle  
 524 size.

Arrangement mode	Side length	Porosity (%)	Specific surface area
Cube	$2d$	47.60	3.142
Hexahedron	$1.577d$	43.30	3.402

525 However, the structure of natural porous media is much more complex and  
 526 heterogeneous than what has been shown in Figure 16, so it is difficult to quantitatively  
 527 describe the effect of sorting degree and arrangement on seepage law.



528

529

Fig. 17. Variation of  $A$  with  $n$  of six gravels with different particle sizes.

530

531

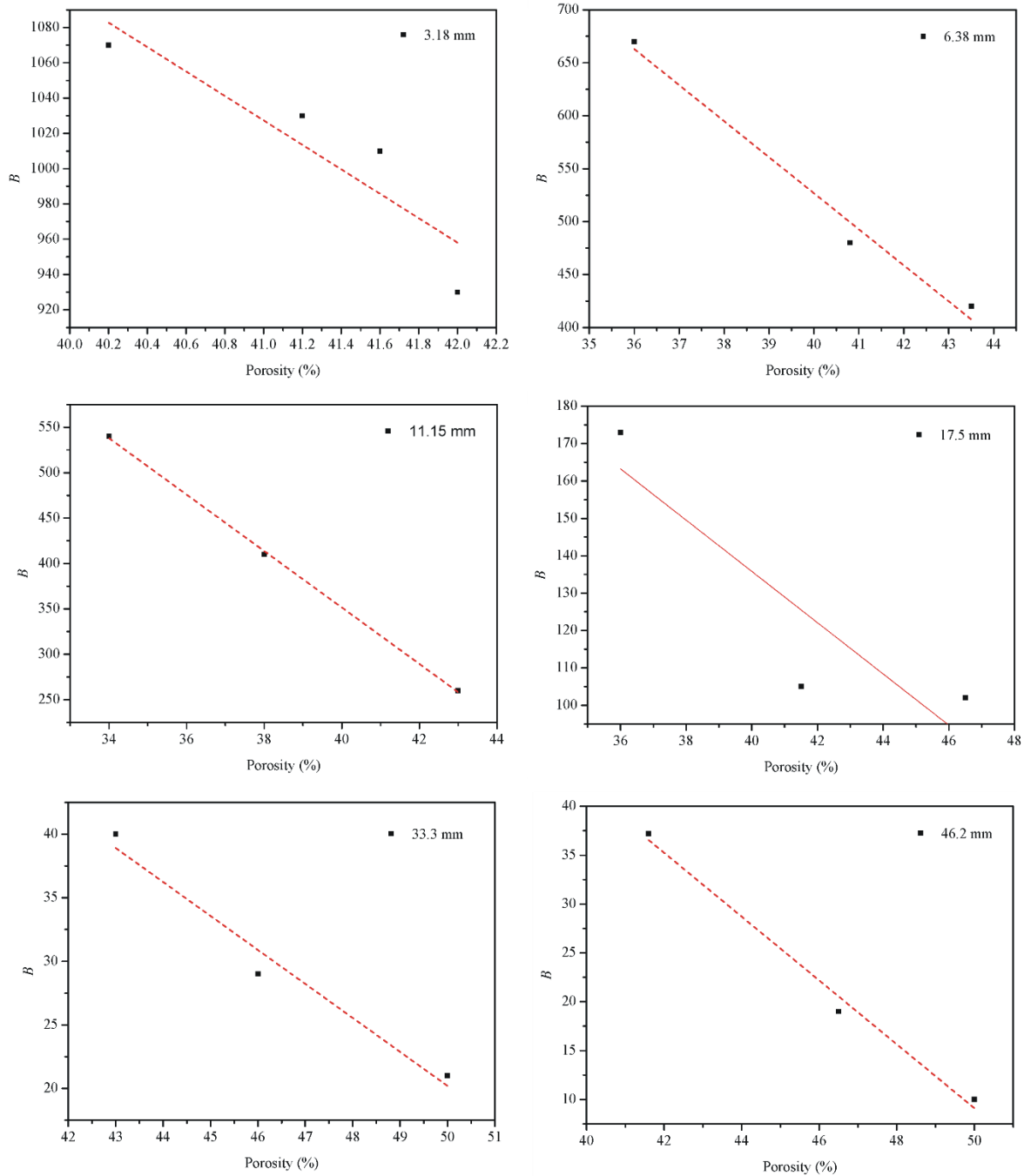
532

533

534

In view of this, we can use a macro parameter porosity ( $n$ ) to reveal the effect of sorting degree and arrangement on seepage coefficient. In order to verify the correctness of the above analysis results, we selected the seepage experiment results of [Niranjan \(1973\)](#) for further validation. [Niranjan \(1973\)](#) chose gravel of the same size but different porosity and carried out seepage experiments. We selected the experimental results of six different particle sizes

535 with 3.18 mm, 6.38 mm, 11.15 mm, 17.5 mm, 33.3 mm and 46.2 mm from [Niranjan \(1973\)](#),  
 536 and drew the relationship between coefficient  $A$  and  $B$  and porosity respectively, as shown in  
 537 Fig. 17 and Fig. 18. We can see that the coefficients  $A$  and  $B$  of the six groups of experimental  
 538 data of [Niranjan \(1973\)](#) decrease with the increase of porosity, which is consistent with our  
 539 theoretical analysis of this investigation.



540

541

Fig. 18. Variation of  $B$  with  $n$  of six gravels with different particle sizes.



#### 542 4. Summary and conclusions

543 This study presents experimental results of Forchheimer flow in four different  
544 permeable stones with different mesh sizes, including 24 mesh size (0.71 mm), 46 mesh size  
545 (0.36 mm), 60 mesh size (0.25 mm), 80 mesh size (0.18 mm). The effects of mean pore size  
546 and pore size distribution on the transition of flow regimes (from pre-Darcian to post-Darcian)  
547 are discussed. In addition, the mercury injection experiment is proposed to investigate the  
548 pore distribution of the permeable stones. In addition, the Forchheimer coefficients are  
549 specifically discussed. The main conclusions can be summarized as follows:

550 1) The relationships between specific discharge ( $q$ ) and the "pseudo" hydraulic conductivity  
551 ( $K$ ) (which is computed as a ratio of  $q$  and hydraulic gradient,  $J$ ) of permeable stones show  
552 that deviation from Darcian flow regime is clearly visible. In addition, the critical specific  
553 discharge corresponding to the transition of flow regimes (from pre-Darcian to post-Darcian)  
554 increases with the increase of mean particle size.

555 2) When the specific discharge is small, only a small fraction of the water flowing through  
556 the pores. The rest of the water adheres to the surface of the solid particles (immobile),  
557 partially blocking the flow pathways. As the specific discharge increases, more water  
558 becomes mobile and participates in flow. Hence, the "pseudo" hydraulic conductivity  
559 increases with the increase of specific discharge. When the specific discharge increases to the  
560 critical specific discharge ( $q_c$ ), the "pseudo" hydraulic conductivity is maximized, and then it  
561 begins to decrease as the specific discharge continues to increase.

562 3) The mercury injection experiment results show that the mercury injection curve can be  
563 divided into three segments. The beginning and end segments of the mercury injection curve  
564 of the four permeable stones with different particle sizes are very gentle, while the main (or  
565 intermediate) mercury injection curve is steep, indicating that the pore size distribution falls  
566 within a narrow range, and the proportions of large pores and small pores are relatively small.

567 4) The porosity decreases as the mean particle size of permeable stone increases while the  
568 mean pore diameter increases. And the porosity can reflect the influence of particle diameter,  
569 sorting degree and arrangement mode of porous medium on seepage parameters. The larger  
570 porosity leads to the smaller coefficients  $A$  and  $B$  under the condition of the same particle size.  
571 5) The coefficient  $A$  is linearly related to  $1/d^2$  and the relationship between coefficient  $A$  and  
572  $1/d^2$  is given as  $A = 0.0025(1/d^2) + 0.003$ . The coefficient  $B$  is not linearly related to  $1/d$ ,  
573 instead it is quadratic related to  $1/d$  as  $B = 1.14E-06(1/d)^2 - 1.26E-06(1/d)$ . The particle  
574 shape and arrangement of permeable stone have imposed great influences on the seepage  
575 parameters.

576 **Notation**

577	$q$	The specific discharge, m/d.
578	$K$	The Hydraulic conductivity, m/d.
579	$J$	The dimensionless parameter defined as hydraulic gradient.
580	$A$	The Forchheimer equation coefficient (viscous force item), $\text{sm}^{-1}$ .
581	$B$	The Forchheimer equation coefficient (Inertia force item), $\text{s}^2\text{m}^{-2}$ .
582	$P_c$	The capillary force, $Pa$ .
583	$P_{50}$	The corresponding pressure value when the saturation reaches 50%, $MPa$ .
584	$P_A, P_B, P_C$	The pressure corresponding to different stages on mercury injection curve, $MPa$ .
585	$\sigma$	The solid-liquid interfacial tension.
586	$\theta$	The wet angle between the liquid and the solid surface.
587	$r$	The radius of curvature in capillary, mm.
588	$d$	The particle size, mm.

589  $d_{50}$  The mean particle sizes (50% by weight), mm.

590  $R_m$  The mean pore diameter,  $\mu m$ .

591  $R_{50}$  The pore diameter corresponding to the median pressure  $P_{50}$ ,  $\mu m$ .

592  $H$  The height of the peak of the mercury injection curve.

593  $x_c$  The abscissa corresponding to the peak of the curve (the pore size).

594  $w$  The standard variance.

595  $n$  The porosity.

596  $J_n$  The viscous force-related component.

597  $J_r$  The inertia force-related component.

598 **Authors contributions**

599 Zhongxia Li: Experiment, Writing original draft. Junwei Wan: Methodology,  
600 Conceptualization. Tao Xiong: Data curation, Investigation, Experiment. Hongbin Zhan:  
601 Methodology, Writing, Review & Editing. Linqing He: Experiment, Methodology. Kun  
602 Huang: Funding acquisition, Investigation

603 **Competing interests**

604 The authors declare that they have no conflict of interest.

605 **Acknowledgements**

606 This study was supported by the National Natural Science Foundation of China (Grant  
607 Nos. 41402204), the National Key Research and Development Program of China  
608 (No. 2018YFC0604202) and the Fundamental Research Funds for National Universities,  
609 China University of Geosciences (Wuhan). Thank Zhongzhi Shen of China University of  
610 Geosciences for his great help in developing the experimental set up. And the authors want to

611 express their sincere appreciation of the constructive comments made by the three  
612 anonymous reviewers and Associate Editor for improving the quality of the manuscript.

## 613 **References**

- 614 Alvarez, A. E., Mahmoud, E., Martin, A. E., Masad, E., and Estakhri, C.: Stone-on-stone contact of permeable  
615 friction course mixtures, *Journal of Materials in Civil Engineering*, 22, 1129-1138,  
616 [https://doi.org/10.1061/\(ASCE\)MT.1943-5533.0000117](https://doi.org/10.1061/(ASCE)MT.1943-5533.0000117), 2010.
- 617 Anovitz, L. M. and Cole, D. R.: Characterization and Analysis of Porosity and Pore Structures, *Reviews in*  
618 *Mineralogy and Geochemistry*, 80, 61-164, <https://doi.org/10.2138/rmg.2015.80.04>, 2015.
- 619 Bear, J.: *Dynamics of Fluids in Porous Media*, American Elsevier Pub. Co., New York, N.Y., and  
620 Amsterdam, 1972.
- 621 Beavers, G. S., Sparrow, E., and Rodenz, D. E.: Influence of Bed Size on the Flow Characteristics and Porosity  
622 of Randomly Packed Beds of Spheres, *Journal of Applied Mechanics*, 40, 655-660,  
623 <https://doi.org/10.1115/1.3423067>, 1972.
- 624 Blick, E.: Capillary-Orifice Model for High-Speed Flow through Porous Media, *Industrial Engineering*  
625 *Chemistry Process Design Development*, 5, 90-94, <https://doi.org/10.1021/i260017a019>, 1966.
- 626 Bu, S., Yang, J., Dong, Q., and Wang, Q.: Experimental study of transition flow in packed beds of spheres with  
627 different particle sizes based on electrochemical microelectrodes measurement, *Applied Thermal Engineering*,  
628 73, 1525-1532, 2014.
- 629 Darcy, H.: *Recherches expérimentales relatives au mouvement de l'eau dans les tuyaux*, Impr. Impériale, Paris,  
630 France, 1857.
- 631 Dejam, M., Hassanzadeh, H., and Chen, Z.: Pre-Darcy flow in porous media, *Water Resources Research*, 53,  
632 8187-8210, <https://doi.org/10.1002/2017WR021257>, 2017.
- 633 Dudgeon, C. R.: An experimental study of the flow of water through coarse granular media, *La Houille Blanche*,  
634 785-801, <https://doi.org/10.1051/lhb/1966049>, 1966.
- 635 Dybbs, A. and Edwards, R.: A new look at porous media fluid mechanics—Darcy to turbulent, in: *Fundamentals*  
636 *of transport phenomena in porous media*, Springer, 199-256, 1984.
- 637 Ergun, S.: Fluid flow through packed columns, *Chemical Engineering Progress*, 89-94,  
638 [https://doi.org/10.1016/0009-2509\(53\)80048-5](https://doi.org/10.1016/0009-2509(53)80048-5), 1952.
- 639 Fancher, G. H. and Lewis, J. A.: Flow of simple fluids through porous materials, *Industrial & Engineering*  
640 *Chemistry*, 25, 1139-1147, <https://doi.org/10.1021/ie50286a020>, 1933.
- 641 Fetter, C. W.: *Applied Hydrogeology: International Edition*, Prentice Hall, Pearson, Engelwood Cliffs, 2001.
- 642 Forchheimer, P.: *Wasserbewegung durch boden*, Z. Ver. Deutsch, Ing., 45, 1728-1782, 1901.
- 643 Geertsma, J.: Estimating the Coefficient of Inertial Resistance in Fluid Flow Through Porous Media, *Society of*  
644 *Petroleum Engineers Journal*, 14, 445-450, <https://doi.org/10.2118/4706-PA>, 1974.
- 645 Guan, X., Wang, J., and Xiao, F.: Sponge city strategy and application of pavement materials in sponge city,  
646 *Journal of Cleaner Production*, 127022, <https://doi.org/10.1016/j.jclepro.2021.127022>, 2021.
- 647 Hall, P. L., Mildner, D., and Borst, R. L.: Small-angle scattering studies of the pore spaces of shaly rocks,  
648 *Journal of Geophysical Research Atmospheres*, 91, 2183-2192, <https://doi.org/10.1029/JB091iB02p02183>, 1986.
- 649 Han, D., Wei, L., and Zhang, J.: Experimental study on performance of asphalt mixture designed by different

650 method, *Procedia engineering*, 137, 407-414, <https://doi.org/10.1016/j.proeng.2016.01.275>, 2016.

651 Harlan, J., Picot, D., Loll, P., and Garavito, R.: Calibration of size-exclusion chromatography: use of a double  
652 Gaussian distribution function to describe pore sizes, *Analytical biochemistry*, 224, 557-563,  
653 <https://doi.org/10.1006/abio.1995.1087>, 1995.

654 Hea, X. and Zhangb, Z.: Microscopic Pore Structural Characteristics in Coal Particles, International Conference  
655 on Material, Guangzhou, China,

656 Huang, K.: Exploration of the basic seepage equation in porous media, PhD dissertation, 2012.

657 Huang, K., Wan, J., Chen, C., Linqing, H., Mei, W., and Zhang, M.: Experimental investigation on water flow in  
658 cubic arrays of spheres, *Journal of Hydrology*, 492, 61-68, <https://doi.org/10.1016/j.jhydrol.2013.03.039>, 2013.

659 Irmay, S.: Theoretical models of flow through porous media, RILEM Symp. Transfer of Water in porous media,  
660 Paris, Bull. RILEM, 29, 37-43, 1964.

661 Izbash, S.: *O Filtracii V Kropnozernstom Materiale*, Leningrad, USSR, 1931.

662 Javadi, M., Sharifzadeh, M., Shahriar, K., and Mitani, Y.: Critical Reynolds number for nonlinear flow through  
663 rough walled fractures: The role of shear processes, *Water Resources Research*, 50, 1789-1804,  
664 <https://doi.org/10.1002/2013WR014610>, 2014.

665 Jeon, H., Cho, H., Kim, J., and Sung, B.: Non-Gaussian rotational diffusion in heterogeneous media, *Physical  
666 Review E Statistical Nonlinear & Soft Matter Physics*, 90, 042105, <https://doi.org/10.1103/PhysRevE.90.042105>,  
667 2014.

668 Kadlec, R. H. and Knight, R. L.: *Treatment Wetlands*, Lewis Pub, Boca Raton, 1996.

669 Kate, J. M. and Gokhale, C. S.: A simple method to estimate complete pore size distribution of rocks,  
670 *Engineering Geology*, 84, 48-69, <https://doi.org/10.1016/j.enggeo.2005.11.009>, 2006.

671 Koch, D. and Ladd, A.: Moderate Reynolds number flows through periodic and random arrays of aligned  
672 cylinders, *Journal of Fluid Mechanics*, 349, 31-66, <https://doi.org/10.1017/S002211209700671X>, 1996.

673 Kovács, G.: *Seepage Hydraulics, Development in Water Sciences*. Elsevier: New York, 1981.

674 Latifi, M., Midoux, N., Storck, A., and Gence, J.: The use of micro-electrodes in the study of the flow regimes in  
675 a packed bed reactor with single phase liquid flow, *Chemical engineering science*, 44, 2501-2508, 1989.

676 Li, Q., Wang, F., Yu, Y., Huang, Z., Li, M., and Guan, Y. J. J. o. E. M.: Comprehensive performance evaluation  
677 of LID practices for the sponge city construction: a case study in Guangxi, China, *Journal of Environmental  
678 Management*, 231, 10-20, <https://doi.org/10.1016/j.jenvman.2018.10.024>, 2019a.

679 Li, Z., Wan, J., Huang, K., Chang, W., and He, Y.: Effects of particle diameter on flow characteristics in sand  
680 columns, *International Journal of Heat & Mass Transfer*, 104, 533-536,  
681 <https://doi.org/10.1016/j.ijheatmasstransfer.2016.08.085>, 2017.

682 Li, Z., Wan, J., Zhan, H., Cheng, X., Chang, W., and Huang, K.: Particle size distribution on Forchheimer flow  
683 and transition of flow regimes in porous media, *Journal of Hydrology*, 574, 1-11,  
684 <https://doi.org/10.1016/j.jhydrol.2019.04.026>, 2019b.

685 Lindquist, E.: On the flow of water through porous soil, Premier Congres des grands barrages (Stockholm)1933.

686 Lindquist, W. B., Venkatarangan, A., Dunsmuir, J., and Wong, T. F.: Pore and throat size distributions measured  
687 from synchrotron X-ray tomographic images of Fontainebleau sandstones, *Journal of Geophysical Research  
688 Solid Earth*, 105, 21509-21527, <https://doi.org/10.1029/2000JB900208>, 2000.

689 Maalal, O., Prat, M., Peinador, R., and Lasseux, D.: Determination of the throat size distribution of a porous  
690 medium as an inverse optimization problem combining pore network modeling and genetic and hill climbing  
691 algorithms, *Physical Review E*, 103, 023303, <https://doi.org/10.1103/PhysRevE.103.023303>, 2021.

692 Macdonald, I., El-Sayed, M., Mow, K., and Dullien, F.: Flow through porous media-the Ergun equation revisited,  
693 Industrial & Engineering Chemistry Fundamentals, 18, 199-208, <https://doi.org/10.1021/i160071a001>, 1979.

694 Moutsopoulos, K. N., Papaspyros, I. N., and Tsihrintzis, V. A.: Experimental investigation of inertial flow  
695 processes in porous media, Journal of hydrology, 374, 242-254, <https://doi.org/10.1016/j.jhydrol.2009.06.015>,  
696 2009.

697 Niranjana, H.: Non-Darcy flow through porous media, M.S., dissertation, ITT, Kanpur, India, 1973.

698 Panfilov, M. and Fourar, M.: Physical splitting of nonlinear effects in high-velocity stable flow through porous  
699 media, Advances in Water Resources, 29, 30-41, <https://doi.org/10.1016/j.advwatres.2005.05.002>, 2006.

700 Pittman, E. D.: Relationship of porosity and permeability to various parameters derived from mercury injection-  
701 capillary pressure curves for sandstone (1), AAPG bulletin, 76, 191-198, [https://doi.org/10.1306/BDF87A4-  
702 1718-11D7-8645000102C1865D](https://doi.org/10.1306/BDF87A4-1718-11D7-8645000102C1865D), 1992.

703 Prowell, B. D., Allen Cooley Jr, L., and Schreck, R. J.: Virginia's experience with 9.5-mm nominal-maximum-  
704 aggregate-size stone matrix asphalt, Transportation research record, 1813, 133-141,  
705 <https://doi.org/10.3141/1813-16>, 2002.

706 Rezaee, R., Saeedi, A., and Clennell, B.: Tight gas sands permeability estimation from mercury injection  
707 capillary pressure and nuclear magnetic resonance data, Journal of Petroleum Science and Engineering, 88, 92-  
708 99, <https://doi.org/10.1016/j.petrol.2011.12.014>, 2012.

709 Rijfkoogel, L. S., Ghanbarian, B., Hu, Q., and Liu, H. H.: Clarifying pore diameter, pore width, and their  
710 relationship through pressure measurements: A critical study, Marine and Petroleum Geology, 107, 142-148,  
711 <https://doi.org/10.1016/j.marpetgeo.2019.05.019>, 2019.

712 Scheidegger, A.: The physics of flow through porous media,  
713 Scheidegger, A. E.: On the stability of displacement fronts in porous media: a discussion of the muskat-  
714 aronofsky model, Canadian Journal of Physics, 38, 153-162, <https://doi.org/10.1139/p60-017>, 1960.

715 Scheidegger, A. E.: The physics of flow through porous media, University of Toronto Press,  
716 <https://doi.org/10.3138/9781487583750>, 2020.

717 Schmitt, M., Fernandes, C. P., da Cunha Neto, J. A., Wolf, F. G., and dos Santos, V. S.: Characterization of pore  
718 systems in seal rocks using nitrogen gas adsorption combined with mercury injection capillary pressure  
719 techniques, Marine and Petroleum Geology, 39, 138-149, <https://doi.org/10.1016/j.marpetgeo.2012.09.001>, 2013.

720 Schneebeil, G.: Experiences sur la limite de validite de la loi de Darcy et l'apparition de la turbulence dans un  
721 ecoulement de filtration, La Huille Blanche, 2, 141-149, <https://doi.org/10.1051/lhb/1955030>, 1955.

722 Sedghi-Asl, M., Rahimi, H., and Salehi, R.: Non-Darcy Flow of Water Through a Packed Column Test,  
723 Transport in Porous Media, 101, 215-227, <https://doi.org/10.1007/s11242-013-0240-0>, 2014.

724 Seguin, D., Montillet, A., Comiti, J., and Huet, F.: Experimental characterization of flow regimes in various  
725 porous media—II: Transition to turbulent regime, Chemical engineering science, 53, 3897-3909, 1998.

726 Shi, W., Yang, T., and Yu, S.: Experimental Investigation on Non-Darcy Flow Behavior of Granular Limestone  
727 with Different Porosity, Journal of Hydrologic Engineering, 25, 06020004,  
728 [https://doi.org/10.1061/\(ASCE\)HE.1943-5584.0001966](https://doi.org/10.1061/(ASCE)HE.1943-5584.0001966), 2020.

729 Sidiropoulou, M. G., Moutsopoulos, K. N., and Tsihrintzis, V.: Determination of Forchheimer equation  
730 coefficients a and b, Hydrological Processes, 21, 534-554, <https://doi.org/10.1002/hyp.6264>, 2007.

731 Skjetne, E., Hansen, A., and Gudmundsson, J.: High-velocity flow in a rough fracture, Journal of Fluid  
732 Mechanics, 383, 1-28, <https://doi.org/10.1017/S0022112098002444>, 1999.

733 Soni, J., Islam, N., and Basak, P.: An experimental evaluation of non-Darcian flow in porous media, Journal of

734 Hydrology, 38, 231-241, [https://doi.org/10.1016/0022-1694\(78\)90070-7](https://doi.org/10.1016/0022-1694(78)90070-7), 1978.

735 Souto, H. P. A. and Moyne, C.: Dispersion in two-dimensional periodic porous media. Part I. Hydrodynamics,  
736 Physics of Fluids, 9, 2243-2252, <https://doi.org/10.1063/1.869365>, 1997.

737 Suo, Z., Bao, X., Nie, L., Yan, Q., and Qi, K.: Optimization Design of Mix Proportion of Large Stone Permeable  
738 Mixture Based on Target Air Voids, Buildings, 11, 514, <https://doi.org/10.3390/buildings11110514>, 2021.

739 Swartzendruber, D.: Modification of Darcy's law for the flow of water in soils, Soil Science, 93, 22-29,  
740 <https://doi.org/10.1097/00010694-196201000-00005>, 1962a.

741 Swartzendruber, D.: Non-Darcy flow behavior in liquid-saturated porous media, Journal of Geophysical  
742 Research, 67, 5205-5213, <https://doi.org/10.1029/JZ067i013p05205>, 1962b.

743 Van Lopik, J. H., Zazai, L., Hartog, N., and Schotting, R.: Nonlinear Flow Behavior in Packed Beds of Natural  
744 and Variably Graded Granular Materials, Transport in Porous Media, 131, 957-983,  
745 <https://doi.org/10.1007/s11242-019-01373-0>, 2019.

746 Van Lopik, J. H., Snoeijers, R., van Dooren, T. C. G. W., Raoof, A., and Schotting, R. J.: The Effect of Grain  
747 Size Distribution on Nonlinear Flow Behavior in Sandy Porous Media, Transport in Porous Media, 120, 1-30,  
748 <https://doi.org/10.1007/s11242-017-0903-3>, 2017.

749 Wang, J., Ng, P.-L., Gong, Y., Su, H., and Du, J.: Experimental Study of Low Temperature Performance of  
750 Porous Asphalt Mixture, Applied Sciences, 11, 4029, <https://doi.org/10.3390/app11094029>, 2021.

751 Ward, J. C.: Turbulent Flow in Porous Media, Journal of Hydraulic Engineering, 90, 1-12,  
752 [http://dx.doi.org/10.1016/S0301-9322\(02\)00051-4](http://dx.doi.org/10.1016/S0301-9322(02)00051-4), 1964.

753 Washburn, E. W.: The Dynamics of Capillary Flow, Physical Review, 17, 273-283,  
754 <https://doi.org/10.1103/PhysRev.17.273>, 1921.

755 Wright, D.: Nonlinear Flow Through Granular Media, Journal of Hydraulic Engineering, 94, 851-872,  
756 <https://doi.org/10.1061/JYCEAJ.0001858>, 1968.

757 Xie, H. and Watson, D. E.: Determining air voids content of compacted stone matrix asphalt mixtures,  
758 Transportation research record, 1891, 203-211, <https://doi.org/10.3141/1891-24>, 2004.

759 Xu, C. and Torres-Verdín, C.: Pore System Characterization and Petrophysical Rock Classification Using a  
760 Bimodal Gaussian Density Function, Mathematical Geosciences, 45, 753-771, <https://doi.org/10.1007/s11004-013-9473-2>, 2013.

761  
762 Yang, B., Yang, T., Xu, Z., Liu, H., Yang, X., and Shi, W.: Impact of Particle-Size Distribution on Flow  
763 Properties of a Packed Column, Journal of Hydrologic Engineering, 24, 04018070,  
764 [https://doi.org/10.1061/\(ASCE\)HE.1943-5584.0001735](https://doi.org/10.1061/(ASCE)HE.1943-5584.0001735), 2019.

765 Yu, T., Liu, D., Zhang, H., and Wang, H.: Influence of pore water phase change on service performance for  
766 permeable pavement in Sponge City, Water Science and Technology, 84, 3769-3779,  
767 <https://doi.org/10.2166/wst.2021.459>, 2021.

768 Zeng, Z. and Grigg, R.: A criterion for non-Darcy flow in porous media, Transport in porous media, 63, 57-69,  
769 <https://doi.org/10.1007/s11242-005-2720-3>, 2006.

770 Zhen-hua, MIN, and, Min, CAO, and, Shu, ZHANG, and, and Xiu-dan: Effect of precursor on the pore structure  
771 of carbon foams, New Carbon Materials, 22, 75-79, [https://doi.org/10.1016/S1872-5805\(07\)60009-2](https://doi.org/10.1016/S1872-5805(07)60009-2), 2007.

772 Zhihong, L. I., Jihong, S., Dong, W. U., Yuhan, S., Liu, Y. I., Wenjun, S., and Baozhong, D.: Determination of  
773 average pore diameter of SiO<sub>2</sub> xerogels by small angle X-ray scattering, ACTA Physica sinica, 49, 1312-1315,  
774 <https://doi.org/10.3321/j.issn:1000-3290.2000.07.020>, 2000.

775 Zhou, H., Fang, Y.-g., Chen, M., Gu, R.-g., and Li, W.: Experimental and analytical study on electro-osmosis in

776 low-permeability soil considering the pore size effect, *Geotechnique*, 71, 141-152,  
777 <https://doi.org/10.1680/jgeot.18.p.362>, 2019.  
778